

# Does black hole growth depend fundamentally on host-galaxy compactness?

Q. Ni,<sup>1,2★</sup> G. Yang<sup>1,2★</sup>, W. N. Brandt,<sup>1,2,3</sup> D. M. Alexander,<sup>4</sup> C.-T. J. Chen<sup>5</sup>,  
B. Luo,<sup>6,7,8</sup> F. Vito<sup>9,10</sup> and Y. Q. Xue<sup>11,12</sup>

<sup>1</sup>525 Davey Lab, Department of Astronomy and Astrophysics, The Pennsylvania State University, University Park, PA 16802, USA

<sup>2</sup>Institute for Gravitation and the Cosmos, The Pennsylvania State University, University Park, PA 16802, USA

<sup>3</sup>104 Davey Laboratory, Department of Physics, The Pennsylvania State University, University Park, PA 16802, USA

<sup>4</sup>Centre for Extragalactic Astronomy, Department of Physics, Durham University, South Road, Durham DH1 3LE, UK

<sup>5</sup>Marshall Space Flight Center, Huntsville, AL 35811, USA

<sup>6</sup>School of Astronomy and Space Science, Nanjing University, Nanjing 210093, China

<sup>7</sup>Key Laboratory of Modern Astronomy and Astrophysics, Nanjing University, Ministry of Education, Nanjing 210093, China

<sup>8</sup>Collaborative Innovation Center of Modern Astronomy and Space Exploration, Nanjing 210093, China

<sup>9</sup>Instituto de Astrofísica and Centro de Astroingeniería, Facultad de Física, Pontificia Universidad Católica de Chile, Casilla 306, Santiago 22, Chile

<sup>10</sup>Chinese Academy of Sciences South America Center for Astronomy, National Astronomical Observatories, CAS, Beijing 100012, China

<sup>11</sup>CAS Key Laboratory for Research in Galaxies and Cosmology, Department of Astronomy, University of Science and Technology of China, Hefei 230026, China

<sup>12</sup>School of Astronomy and Space Science, University of Science and Technology of China, Hefei 230026, China

Accepted 2019 September 11. Received 2019 September 11; in original form 2019 June 13

## ABSTRACT

Possible connections between central black hole (BH) growth and host-galaxy compactness have been found observationally, which may provide insight into BH–galaxy coevolution: compact galaxies might have large amounts of gas in their centres due to their high mass-to-size ratios, and simulations predict that high central gas density can boost BH accretion. However, it is not yet clear if BH growth is fundamentally related to the compactness of the host galaxy, due to observational degeneracies between compactness, stellar mass ( $M_*$ ) and star formation rate (SFR). To break these degeneracies, we carry out systematic partial-correlation studies to investigate the dependence of sample-averaged BH accretion rate ( $\overline{\text{BHAR}}$ ) on the compactness of host galaxies, represented by the surface-mass density,  $\Sigma_e$ , or the projected central surface-mass density within 1 kpc,  $\Sigma_1$ . We utilize 8842 galaxies with  $H < 24.5$  in the five CANDELS fields at  $z = 0.5$ – $3$ . We find that  $\overline{\text{BHAR}}$  does not significantly depend on compactness when controlling for SFR or  $M_*$  among bulge-dominated galaxies and galaxies that are not dominated by bulges, respectively. However, when testing is confined to star-forming galaxies at  $z = 0.5$ – $1.5$ , we find that the  $\overline{\text{BHAR}}$ – $\Sigma_1$  relation is not simply a secondary manifestation of a primary  $\overline{\text{BHAR}}$ – $M_*$  relation, which may indicate a link between BH growth and the gas density within the central 1 kpc of galaxies.

**Key words:** galaxies: active – galaxies: evolution – galaxies: nuclei – X-rays: galaxies.

## 1 INTRODUCTION

Understanding the connections between supermassive black holes (BHs) and their host galaxies has been an essential problem for the past two decades. It is well established that BH mass ( $M_{\text{BH}}$ ) is correlated with the stellar mass, luminosity, and velocity dispersion of the host-galaxy bulge in the local Universe (e.g. Magorrian et al. 1998; Kormendy & Ho 2013), suggesting the coevolution of BHs and their host galaxies. However, the fundamental link between BH

accretion and galaxy growth is still not well understood, and remains one of the most debated issues in astrophysics (e.g. Mullaney et al. 2011; Chen et al. 2013; Hickox et al. 2014; Yang et al. 2017, 2018a,b, 2019; Aird, Coil & Georgakakis 2018). Researchers have investigated the relations between different galaxy properties and BH growth to determine what drives BH–galaxy coevolution, and both star formation rate (SFR; which partly traces the total amount of cold gas available) and stellar mass ( $M_*$ ; which indicates the potential wells of galaxies) have been found to relate to BH growth.

To identify the fundamental link in BH–galaxy coevolution, one promising avenue is to investigate the relation between BH growth and host-galaxy compactness, which, nevertheless, has not

\* E-mail: qxn1@psu.edu (QN); gyang206265@gmail.com (GY)

been conducted in detail. Compactness can be represented by the surface-mass density,  $\Sigma_e$ ;  $\Sigma_e = 0.5M_*/\pi r_e^2$ , where  $r_e$  is the effective radius of the galaxy within which half of the total light is emitted (e.g. Barro et al. 2017; Kocevski et al. 2017). This widely adopted measurement of compactness measures the mass-to-size ratio in the central 50% of a galaxy by its definition, thus assessing the compactness globally. Alternatively, compactness can be represented by the central surface-mass density within 1 kpc,  $\Sigma_1$ ;  $\Sigma_1 = M_*( < 1 \text{ kpc})/\pi(1 \text{ kpc})^2$ , where  $M_*( < 1 \text{ kpc})$  is the stellar mass enclosed in the central 1 kpc of a galaxy. It has been suggested that the central stellar density within 1 kpc is more effective at connecting galaxy morphology and star formation activity when compared with surface-mass density (e.g. Cheung et al. 2012; van Dokkum et al. 2014; Whitaker et al. 2017; Lee et al. 2018). Thus,  $\Sigma_1$  might also be a more effective parameter connecting galaxy morphology and BH growth compared with  $\Sigma_e$ . It is plausible that large amounts of gas are located within the nuclear regions of some compact galaxies (particularly, those that are actively star-forming) due to their high mass-to-size ratios, and simulations predict that high central gas density can boost BH accretion (e.g. Wellons et al. 2015; Habouzit et al. 2019). Recent galaxy evolution simulations and models also predict a dissipative-contraction process (i.e. wet compaction event; e.g. Dekel & Burkert 2014; Zolotov et al. 2015; Tacchella et al. 2016a,b) that triggers a compact starburst, which can also trigger concurrent growth of the central BH. In this paper, we will sometimes speak of compactness,  $\Sigma$ , generally, where  $\Sigma$  could mean either  $\Sigma_e$  or  $\Sigma_1$  (i.e. ‘ $\Sigma$ ’ should be interpreted as ‘ $\Sigma_e/\Sigma_1$ ’).

In the local Universe, several overmassive BH ‘monsters’ have been found in notably compact galaxies, which have  $M_{\text{BH}}$  values significantly larger than those expected from the relation with bulge mass (e.g. Kormendy & Ho 2013; Ishibashi & Fabian 2017). Adding  $r_e$  as an additional parameter can indeed tighten the local relation between  $M_{\text{BH}}$  and the stellar mass or velocity dispersion of the host-galaxy bulge (e.g. Marconi & Hunt 2003; Beifiori et al. 2012).

Possible connections between compactness and BH growth have been found with the great depth and high angular resolution of the *HST* CANDELS survey (e.g. Grogin et al. 2011; Koekemoer et al. 2011). Kocevski et al. (2017) found that the AGN fraction among massive compact star-forming galaxies is significantly higher when compared with mass-matched extended star-forming galaxies at  $1.4 < z < 3$ . Rangel et al. (2014) suggested that absorption-corrected AGN X-ray luminosities correlate with the host-galaxy compactness at  $M_* > 10^{10.5} M_\odot$ . While those studies provided important clues about the role of compactness in BH–galaxy coevolution, neither of them could answer the question: is BH growth *fundamentally* linked with the compactness of its host galaxy?

Compactness is correlated with stellar mass by construction, raising questions about which of these quantities is most fundamentally linked to BH growth. Could the observed correlation in Rangel et al. (2014) between compactness and AGN X-ray luminosity simply be a secondary manifestation of a primary correlation between stellar mass and BH growth (e.g. Yang et al. 2017, 2018a)? Also, bulge-dominated galaxies are generally more compact. Could the observed high AGN fraction among compact star-forming galaxies in Kocevski et al. (2017) be a natural consequence of a large amount of BH growth expected among star-forming bulges (e.g. Silverman et al. 2008; Yang et al. 2019)? Or, if compactness is indeed a critical property linked with BH growth, perhaps serving as an indicator of central gas density, could the relation between BH growth and  $M_*$  found in Yang et al. (2017, 2018a) simply be reflecting this linkage? Could the relation between BH growth and SFR among

bulge-dominated galaxies presented in Yang et al. (2019) simply be a manifestation of the predicted compact starburst with concurrent BH growth?

In this paper, we aim to break such observational degeneracies and probe if BH growth is fundamentally related to host-galaxy compactness, by carrying out a systematic partial-correlation (PCOR) study for a large galaxy sample. This systematic investigation will contribute to the overall understanding of BH–galaxy coevolution. This paper is structured as follows. In Section 2, we describe the data-assembly process for this work and define our samples. In Section 3, we perform data analyses and present the results. We discuss our results in Section 4. We summarize our work and discuss future prospects in Section 5.

Throughout this paper, we assume a cosmology with  $H_0 = 70 \text{ km s}^{-1} \text{ Mpc}^{-1}$ ,  $\Omega_M = 0.3$ , and  $\Omega_\Lambda = 0.7$ . A Chabrier initial mass function (Chabrier 2003) is adopted.  $M_*$  is in units of  $M_\odot$ . SFR and black hole accretion rate are in units of  $M_\odot \text{ yr}^{-1}$ .  $\Sigma_e$  and  $\Sigma_1$  are in units of  $M_\odot \text{ kpc}^{-2}$ .  $L_X$  indicates X-ray luminosity at rest-frame 2–10 keV in units of  $\text{erg s}^{-1}$  that has been systematically corrected for absorption (see Section 2.3 for further discussion). Quoted uncertainties are at the  $1\sigma$  (68%) confidence level, unless otherwise stated. We consider two quantities to be significantly different if the significance level of their difference is greater than  $3\sigma$  ( $p$ -value = 0.0027), more stringent than the ‘ $p$ -value < 0.05’ hypothesis testing, which can result in a high rate of false positives (e.g. Benjamin et al. 2018). When multiple independent hypothesis tests are being conducted simultaneously, we use the Bonferroni correction (Bonferroni 1936) to adjust the required significance level corresponding to  $p$ -value =  $0.0027/n$ , where  $n$  is the number of tests. We consider a partial correlation to be significant if its test statistic from the PCOR analyses has a  $p$ -value < 0.0027, which corresponds to a significance level  $> 3\sigma$ . Significant results throughout the paper are marked in bold in the tables.

## 2 DATA AND SAMPLE SELECTION

We perform analyses based on a sample of 8842 galaxies at  $0.5 \leq z < 3$  in the five CANDELS fields, i.e. GOODS-S, GOODS-N, EGS, UDS, and COSMOS (Grogin et al. 2011; Koekemoer et al. 2011). All of these CANDELS fields have deep multiwavelength observations from *HST*, *Spitzer*, *Herschel*, and ground-based telescopes such as Keck, Subaru, and VLT, enabling high-quality measurements of galaxy morphology (see Section 2.1),  $M_*$ , and SFR (see Section 2.2). At the same time, all these fields have deep X-ray observations from *Chandra*, enabling estimation of BH growth utilizing X-ray data (see Section 2.3). We define our sample in Section 2.4, and the sample properties are summarized in Table 1.

### 2.1 Structural and morphology measurements

We adopt the structural measurements in van der Wel et al. (2012)<sup>1</sup> for CANDELS *HST*  $H_{\text{F160W}}$ -selected objects derived utilizing GALFIT (Peng et al. 2002). With background estimated

<sup>1</sup>van der Wel et al. (2012) carry out structural measurements based on CANDELS images processed by the CANDELS team, and van der Wel et al. (2014) perform structural measurements based on CANDELS images processed by the 3D-*HST* team. For the purpose of consistency, we utilize the results in van der Wel et al. (2012). Note that for objects in our sample, structural measurements from van der Wel et al. (2012) and van der Wel et al. (2014) agree well.

**Table 1.** Summary of sample properties. (1) CANDELS field name. (2) Field area in arcmin<sup>2</sup>. (3) Number of galaxies in an  $M_*$ -complete sample. The numbers of galaxies in the  $z = 0.5-1.5/z = 1.5-3$  range are quoted in parentheses. (4) Number of spec- $z$ /photo- $z$  sources. (5) Reference for CANDELS galaxy catalogue. (6) Number of X-ray detected galaxies in the sample. The numbers of X-ray detected galaxies in the  $z = 0.5-1.5/z = 1.5-3$  range are quoted in parentheses. (7) X-ray depth in terms of exposure time. (8) Reference for *Chandra* X-ray catalogue.

Field (1)	Area (arcmin <sup>2</sup> ) (2)	Number of galaxies (3)	Number of spec- $z$ /photo- $z$ (4)	Galaxy reference (5)	Number of X-ray detections (6)	X-ray depth (7)	X-ray reference (8)
GOODS-S	170	1274 (907/367)	643/631	Santini et al. (2015)	284 (182/102)	7 Ms	Luo et al. (2017)
GOODS-N	170	1645 (1216/429)	355/1290	Barro et al. (2019)	203 (133/70)	2 Ms	Xue et al. (2016)
EGS	200	2065 (1361/704)	194/1871	Stefanon et al. (2017)	121 (64/57)	800 ks	Nandra et al. (2015)
UDS	200	1863 (1267/596)	227/1636	Santini et al. (2015)	97 (53/44)	600 ks	Kocevski et al. (2018)
COSMOS	220	1995 (1496/499)	9*/1986	Nayyeri et al. (2017)	48 (29/19)	160 ks	Civano et al. (2016)
Total	960	8842 (6247/2595)	1428/7414	–	753 (461/292)	–	–

\*The latest version of the CANDELS/COSMOS catalogue is mostly based on photo- $z$ .

from GALAPAGOS (Barden et al. 2012) and point-spread functions constructed using the *TinyTim* package (Krist 1995), van der Wel et al. (2012) measured structural properties including total magnitude, effective radius ( $r_e$ ), Sérsic index ( $n$ ), axial ratio, and position angle for all galaxies identified in the CANDELS  $H$ -band mosaics from single-component Sérsic model fits, and quantified the systematic and statistical uncertainties utilizing simulated mosaics (Häussler et al. 2007). The detailed assessments of the uncertainty of structural properties including  $r_e$  and  $n$  are given in table 3 of van der Wel et al. (2012). The CANDELS  $J/H$ -band images reach  $J/H \sim 27-28$ . Thus, even for galaxies with  $H \sim 24-24.5$  (which is the magnitude range for the faintest galaxies selected in our sample; see Section 2.4), the median signal-to-noise ratio is  $\approx 40$ . For objects with  $0.5 \leq z < 1.5$ , we adopt structural measurements from the *HST*  $J$ -band ( $1.25 \mu\text{m}$ ); for objects with  $1.5 \leq z < 3$ , we adopt structural measurements from the *HST*  $H$ -band ( $1.6 \mu\text{m}$ ), thus minimizing the effects of the ‘morphological  $k$ -correction’ with all structural measurements being made in the rest-frame optical consistently.

We utilize the machine-learning-based  $H$ -band morphology measurements in Huertas-Company et al. (2015) for CANDELS galaxies with  $H < 24.5$  to distinguish bulge-dominated galaxies from galaxies that are not dominated by bulges. Since we only utilize these morphological measurements for a basic selection, and the morphological  $k$ -correction is weak in the optical or NIR wavelength range (e.g. Taylor-Mager et al. 2007), our results should not be affected qualitatively by the morphological  $k$ -correction (see section 3.4 of Yang et al. 2019 for details). In this catalogue, probabilities that a hypothetical classifier would have voted for a galaxy having a spheroid ( $f_{\text{sph}}$ ), a disc ( $f_{\text{disc}}$ ), and some irregularities ( $f_{\text{irr}}$ ), being point-like ( $f_{\text{pl}}$ ) and unclassifiable ( $f_{\text{unc}}$ ) are presented.

We note that the UV-to-near-IR spectral energy distributions (SEDs) of most ( $\gtrsim 90\%$ ) X-ray AGNs in these fields are dominated by host-galaxy starlight, and thus their morphological measurements should be reliable (e.g. Luo et al. 2010; Xue et al. 2010; Kocevski et al. 2017; Li et al. 2019).

## 2.2 Redshift, stellar mass, and star formation rate

The redshift, stellar mass ( $M_*$ ), and star formation rate (SFR) used in this paper are identical to those used in Yang et al. (2019). We obtain redshift measurements from the CANDELS catalogues (see Table 1). Spectroscopic redshifts (spec- $z$ ) are adopted when available, and photometric redshifts (photo- $z$ ) are taken for the rest of galaxies (see Table 1). Photo- $z$  values for the CANDELS catalogues are of very high quality: they have  $\sigma_{\text{NMAD}} = 0.018$  and

an outlier fraction of 2% compared with spec- $z$ .<sup>2</sup> The CANDELS catalogues also provide  $M_*$  and SFR measurements from independent teams based on SED-fitting utilizing UV-to-NIR photometric bands. The  $M_*$  and SFR used in this work are the median  $M_*$  and SFR values from the five available teams ( $2a_\tau$ ,  $6a_\tau$ ,  $11a_\tau$ ,  $13a_\tau$ , and  $14a$ ).<sup>3</sup> The  $M_*$  values obtained from SED-fitting are generally robust and insensitive to different parameterizations of the star formation history (e.g. Santini et al. 2015), and there is an overall agreement between different teams. While SED-based SFR values are also generally reliable (see fig. 3 of Yang et al. 2017 for a comparison between SED-based SFR values and SFR values derived from *Herschel* photometry), it has been suggested that the SED-based SFR estimation may underestimate SFR in the high-SFR regime (e.g. Wuyts et al. 2011; Yang et al. 2017), where FIR detections are typically expected. Thus, when robust *Herschel* detections with  $S/N > 3$  are available ( $\approx 27\%$ ; Lutz et al. 2011; Oliver et al. 2012; Magnelli et al. 2013), we calculate SFR from FIR photometry to alleviate this issue (using the reddest available *Herschel* band to avoid possible AGN emission). For galaxies with  $z > 1.5$ , we discard all  $100 \mu\text{m}$  detections to avoid the contamination of hot-dust emission linked with AGN activity at rest frame  $< 40 \mu\text{m}$ . For galaxies in the sample we define in Section 2.4.1, the median rest-frame wavelength of utilized *Herschel* detections is  $\approx 130 \mu\text{m}$ , where the AGN emission has limited contribution to the overall emission (that is dominated by galactic emission; e.g. Stalevski et al. 2016; Zou et al. 2019). The procedures for calculating SFR from FIR flux are detailed in Yang et al. (2017), Yang et al. (2019). Basically, we utilize star-forming galaxy templates in Kirkpatrick et al. (2012) to derive the total infrared luminosity from the FIR flux, and then convert it to SFR with the equation:

$$\frac{\text{SFR}}{M_\odot \text{yr}^{-1}} = 1.09 \times 10^{-10} \frac{L_{\text{IR}}}{L_\odot}. \quad (1)$$

We note that our results do not change qualitatively when using SED-based SFR solely, or perturbing adopted SFR values randomly by 0–0.5 dex (the typical scatter between FIR-based SFR and SED-based SFR; Yang et al. 2017).

<sup>2</sup> $\sigma_{\text{NMAD}}$  is defined as  $1.48 \times \text{median}(\frac{|\Delta z - \text{median}(\Delta z)|}{1 + z_{\text{spec}}})$ , where  $\Delta z$  is the difference between spec- $z$  and photo- $z$ . Outliers are those sources with  $|\Delta z|/(1 + z_{\text{spec}}) > 0.15$ .

<sup>3</sup>For GOODS-N, only three teams are available ( $2a_\tau$ ,  $6a_\tau$ , and  $14a$ ).



### 2.3 Black-hole accretion rate

We calculate sample-averaged BH accretion rate ( $\overline{\text{BHAR}}$ ) contributed by both X-ray detected and undetected sources to cover all BH accretion, thus estimating *long-term average BH growth*. BH accretion has large variability (e.g. Sartori et al. 2018; Yuan et al. 2018) on the relevant BH-growth time-scales ( $\sim 10^{6-8}$  yr) that may hide any BH-galaxy connection within individual objects, making  $\overline{\text{BHAR}}$  an ideal estimator for our study. The inclusion of X-ray undetected sources also enables us to analyse all sources in different CANDELS fields seamlessly with different X-ray depths (see Table 1).

For each X-ray detected source, we calculate  $L_X$  from the X-ray flux reported in the corresponding X-ray catalogue assuming a photon index of  $\Gamma = 1.7$  (e.g. Yang et al. 2016; Liu et al. 2017). Following Yang et al. (2018b), we choose, in order of priority, hard-band (observed-frame 2–7 keV), full-band (observed-frame 0.5–7 keV), or soft-band (observed-frame 0.5–2 keV) flux to minimize X-ray obscuration effects. At  $z = 0.5-3$ , the hard band can probe rest-frame X-ray flux up to 10.5–28 keV, enabling good estimation of  $L_X$  until the column density reaches  $N_H \sim 10^{23} \text{ cm}^{-2}$ . For X-ray detected galaxies in the sample defined in Section 2.4.1,  $\approx 62\%$  of them have hard-band detections; full-band detections are utilized for  $\approx 31\%$  of them; soft-band detections are utilized for  $\approx 7\%$  of them. Utilizing bright X-ray sources in the CDF-S, Yang et al. (2018b) compare the X-ray flux obtained via this scheme of band choice with the absorption-corrected X-ray flux in Luo et al. (2017), and show that the underestimation of X-ray flux due to obscuration in this scheme is typically small ( $\approx 20\%$ ). Following Yang et al. (2019), we increase the X-ray fluxes of our X-ray sources by 20% to account for the systematic effects of obscuration.<sup>4</sup> For X-ray undetected sources, we employ the stacking results from Yang et al. (2019) to estimate their X-ray emission.

With  $L_X$  for each individual X-ray detected source and the average X-ray luminosity for any group of X-ray undetected sources obtained via stacking ( $\overline{L_{X,\text{stack}}}$ ), the average AGN bolometric luminosity for a sample of sources can be calculated as (Yang et al. 2019):

$$\overline{L_{\text{bol}}} = \frac{\sum_{n=0}^{N_{\text{det}}} (L_X - L_{X,\text{XRB}}) k_{\text{bol}}}{N_{\text{det}} + N_{\text{non}}} + \frac{(\overline{L_{X,\text{stack}}} - \overline{L_{X,\text{XRB}}}) N_{\text{non}} \overline{k_{\text{bol}}}}{N_{\text{det}} + N_{\text{non}}}. \quad (2)$$

Here,  $N_{\text{det}}$  and  $N_{\text{non}}$  represent the numbers of X-ray detected and undetected sources in the sample, respectively. The summation in the first term of the numerator is over all X-ray detected galaxies. Note that when deriving  $\overline{L_{X,\text{stack}}}$ , some X-ray undetected galaxies are too close to X-ray sources to be stacked ( $\approx 12\%$ ). However, they are still included when counting  $N_{\text{non}}$ , and thus are appropriately accounted for statistically.  $L_{X,\text{XRB}}$  is the expected luminosity from X-ray binaries (XRBs) for each individual X-ray detected source, and  $\overline{L_{X,\text{XRB}}}$  is the average expected XRB luminosity for the stacked sources.  $L_{X,\text{XRB}}$  and  $\overline{L_{X,\text{XRB}}}$  are obtained from model 269 of Fragos

et al. (2013), which describes XRB X-ray luminosity as a redshift-dependent linear function of  $M_*$  and SFR, utilizing observations at  $z = 0-7$  by Lehmer et al. (2016). XRBs typically contribute  $\approx 10-25\%$  of the total X-ray luminosity in the sample, and thus our analyses should not be affected materially by the uncertainties related to the XRB modelling.  $k_{\text{bol}}$  and  $\overline{k_{\text{bol}}}$  are the  $L_X$ -dependent bolometric corrections at  $L_X - L_{X,\text{XRB}}$  and  $\overline{L_{X,\text{stack}}} - \overline{L_{X,\text{XRB}}}$ , respectively, calculated from the model in Hopkins, Richards & Hernquist (2007) and then multiplied by a factor of 0.7 to reconcile the overestimation due to the double counting of IR reprocessed emission (see footnote 4 of Merloni & Heinz 2013).

Assuming a constant radiative efficiency of  $\epsilon = 0.1$  (e.g. Brandt & Alexander 2015; Yang et al. 2019), we can convert  $\overline{L_{\text{bol}}}$  to  $\overline{\text{BHAR}}$  as

$$\begin{aligned} \overline{\text{BHAR}} &= \frac{(1 - \epsilon) \overline{L_{\text{bol}}}}{\epsilon c^2} \\ &= \frac{1.58 \overline{L_{\text{bol}}}}{10^{46} \text{ erg s}^{-1}} M_{\odot} \text{ yr}^{-1}. \end{aligned} \quad (3)$$

The uncertainties on  $\overline{\text{BHAR}}$  are obtained by bootstrapping the sample 1000 times.

### 2.4 Sample construction

#### 2.4.1 Sample selection

First, we select all  $H < 24.5$  galaxies from the CANDELS *HST*  $H$ -band selected catalogues (Santini et al. 2015; Nayyeri et al. 2017; Stefanon et al. 2017; Barro et al. 2019). We note that all  $H < 24.5$  galaxies have structural and morphological measurements from van der Wel et al. (2012) and Huertas-Company et al. (2015), and thus we should not have any biases due to systematic incompleteness issues when performing sample construction. Then, following Yang et al. (2019), we exclude  $\approx 8\%$  of sources that have  $f_{\text{unc}}$  or  $f_{\text{pt}}$  greater than any of  $f_{\text{sph}}$ ,  $f_{\text{disc}}$ , and  $f_{\text{irr}}$ , to exclude stars, broad-line (BL) AGNs, and spurious detections. We also discard the 79 spectroscopic BL AGNs reported in the literature (Barger et al. 2003; Silverman et al. 2010; Cooper et al. 2012; Newman et al. 2013; Marchesi et al. 2016; Suh et al., in prep.). BL AGNs are excluded since their host-galaxy starlight measurements are typically contaminated by AGN light, significantly affecting the  $M_*$ , SFR, and morphology measurements. Assuming the unified model (e.g. Antonucci 1993; Netzer 2015), we note that the exclusion of BL AGNs will not qualitatively change our results: if BL AGNs are purely AGNs observed at certain orientations (not intercepting the torus), a group of BL AGNs sharing similar host properties should have average X-ray luminosity close to that of a group of type 2 AGNs with the same host properties, and the relative fraction of BL AGNs among all AGNs should not change significantly with host properties. Evidence for the validity of these assumptions to first order is given in Merloni et al. (2014) and Zou et al. (2019). Thus, excluding BL AGNs only decreases a similar fraction of  $\overline{\text{BHAR}}$  for bins and subsamples utilized in Section 3, which should not affect the existence of trends between  $\overline{\text{BHAR}}$  and host properties.

We limit our analyses to an  $M_*$ -complete (corresponding to  $H < 24.5$ ) sample. The limiting  $M_*$  ( $M_{\text{lim}}$ ) for  $H < 24.5$  is displayed in Fig. 1. The  $M_{\text{lim}}$ -redshift curve is derived based on an empirical method (e.g. Ilbert et al. 2013). We first divide our sources into narrow redshift bins with width of  $\Delta z = 0.2$ . For each redshift bin, we calculate  $\log M_{\text{lim}}^{\text{ind}} = \log M_* + 0.4 \times (H - 24.5)$  for individual galaxies in the bin. We then adopt  $M_{\text{lim}}$  as the 90th percentile of the  $M_{\text{lim}}^{\text{ind}}$  distribution for the redshift bin.

<sup>4</sup>Since Yang et al. (2018b) utilized CDF-S X-ray sources above the COSMOS flux limits to assess obscuration, the derived obscuration correction factor should be applicable to bright X-ray sources in all the survey fields in this paper, which contribute most of the accretion power. We have also verified that X-ray detected galaxies in different survey fields utilized in the paper do not have significant differences in the average hardness ratio, demonstrating similar levels of X-ray obscuration.



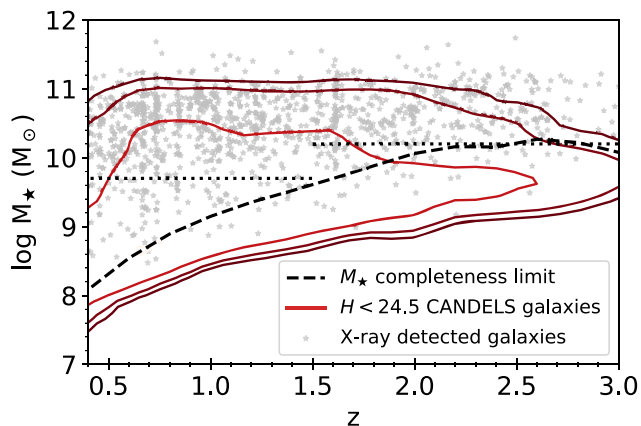


**Figure 1.**  $M_*$  as a function of redshift. The contours encircle 68%, 90%, and 95% of all  $H < 24.5$  galaxies. The grey stars represent X-ray detected sources. The dashed curve indicates the  $M_*$  completeness limit (see Section 2.4.1). The horizontal dotted lines represent our  $M_*$ -completeness cuts for the  $z = 0.5$ – $1.5/1.5$ – $3$  samples selected in Section 2.4.1.

For the studies in Section 3, we divide the objects into two redshift bins:  $0.5 \leq z < 1.5$  and  $1.5 \leq z < 3$ , to probe if the relation between BH growth and host-galaxy compactness changes over cosmic time, and alleviate the influence of the cosmic evolution of compactness (e.g. Barro et al. 2017) in our study. Since the limiting  $M_*$  at  $z = 1.5$  and  $z = 3.0$  are  $\log M_* \approx 9.7$  and  $\log M_* \approx 10.2$  ( $M_*$  in units of  $M_\odot$ ), respectively, we limit our analyses to  $\log M_* > 9.7$  and  $\log M_* > 10.2$  galaxies for the low-redshift and high-redshift bins, respectively. The relatively broad redshift bins are necessary to provide sufficiently large samples for our statistical analyses. We also require `GALFIT_flag` = 0 for the selected galaxies, which includes  $\approx 86\%$  of sources in the  $M_*$ -complete sample. The sample properties are shown in Table 1. Here, `GALFIT_flag` = 0 indicates good quality of the structural

parameters. Sources with `GALFIT_flag` = 1 (9% of the sample) are less certain: they are not necessarily bad fits, but their magnitudes do not fall within the  $3\sigma$  confidence intervals of the magnitude integrated from the light profile measured with GALFIT. We do not include them in the sample to avoid large systematic uncertainties induced by those uncertain measurements, but our results do not vary qualitatively when adding those uncertain sources (see Appendix A). `GALFIT_flag` = 2 indicates sources with one or more parameters reaching the constraint set in GALFIT, which means that the derived structural parameters are not meaningful. `GALFIT_flag` = 3 indicates non-existing results. Thus, we do not consider a flag value of 2 or 3 (5%) for the purpose of this work.

#### 2.4.2 Sample division

For sources in our samples, we classify them as bulge-dominated ( $\approx 25\%$ ; 2212 galaxies) if they have  $f_{\text{sph}} \geq 2/3$ ,  $f_{\text{disc}} < 2/3$ , and  $f_{\text{irr}} < 1/10$ , and those that do not satisfy the criteria (that are not dominated by bulges) are classified into the non-bulge sample (6630 galaxies). This classification approach is supported by visual inspection of the galaxies (see Yang et al. 2019 for more details). Hereafter, we will call the bulge-dominated sample the ‘BD sample’, and the sample of galaxies that are not dominated by bulges the ‘Non-BD sample’ in short.

We use the line that is 1.3 dex below the star formation main sequence derived in Whitaker et al. (2012) at the appropriate redshift and stellar mass to divide star-forming (SF) galaxies from quiescent galaxies. We classify a galaxy as SF if its SFR value is above the line. Our selection of SF galaxies roughly corresponds to galaxies lying above the local minimum in the distribution of SFRs between SF and quiescent galaxies (see Fig. 2). We create a sample of 739 SF galaxies in the BD sample (hereafter ‘SF BD’ in short), and a sample of 5662 SF galaxies in the Non-BD sample (hereafter ‘SF Non-BD’ in short), where cold gas is surely available among galaxies.

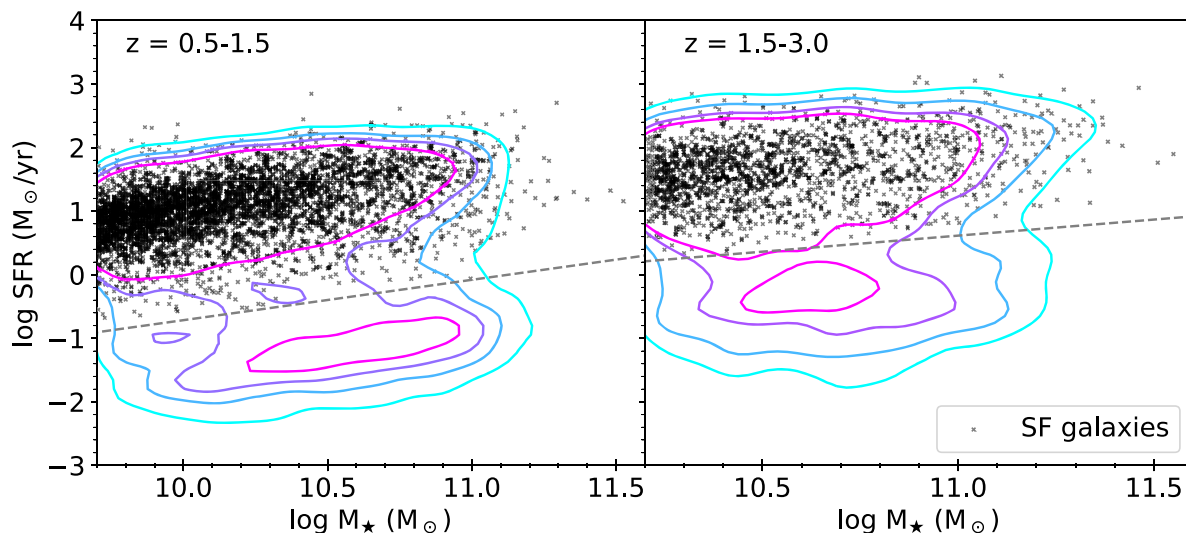


**Figure 2.** SFR versus stellar mass for galaxies in the low-redshift bin (left) and the high-redshift bin (right). The contours encircle 68%, 80%, 90%, and 95% of galaxies in our sample. The black crosses mark the SF galaxies. The grey dashed line in the left-hand or right-hand panel shows the division between SF galaxies and quiescent galaxies at  $z = 0.5/z = 1.5$ . Our selection of SF galaxies roughly corresponds to galaxies lying above the minimum in the distributions of SFRs.

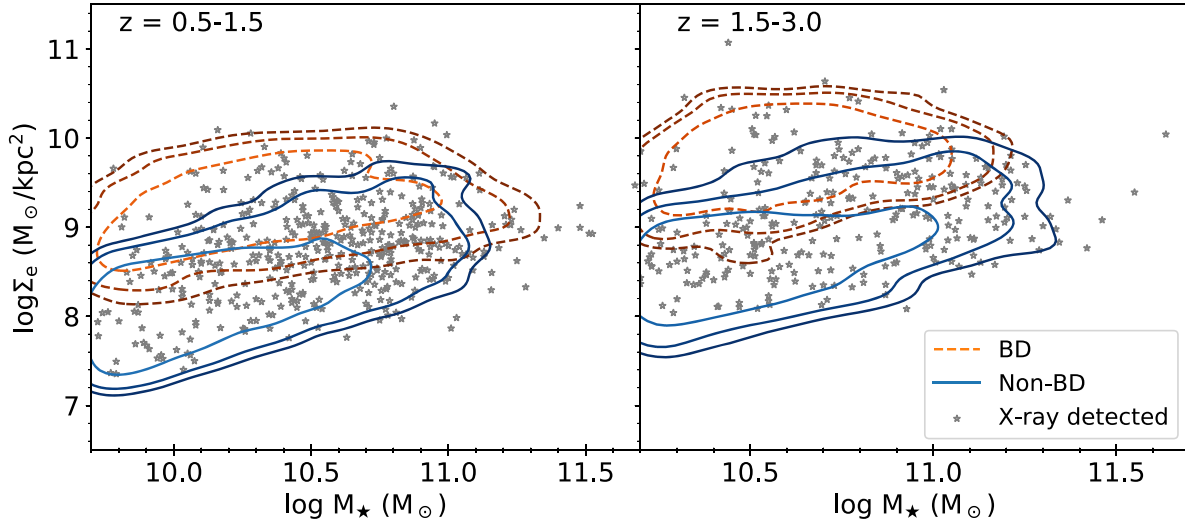


**Figure 3.** Surface-mass density ( $\Sigma_e$ ) versus stellar mass for galaxies in the low-redshift bin (left) and the high-redshift bin (right). The orange dashed contours encircle 68%, 90%, and 95 % of galaxies in the BD sample, and the blue solid contours encircle 68%, 90%, and 95 % of galaxies in the Non-BD sample. The grey stars mark the X-ray detected sources. Galaxies in the BD sample generally have higher  $\Sigma_e$  than galaxies in the Non-BD sample.

#### 2.4.3 Measuring the host-galaxy compactness

To measure the host-galaxy compactness, we first calculate the surface-mass density for galaxies in our sample as  $\Sigma_e = 0.5M_*/\pi r_e^2$ . The effective radius  $r_e$  (measured along a galaxy’s major axis) can be measured with a statistical uncertainty of 20 per cent or better for galaxies with  $H \lesssim 24.5$  (van der Wel et al. 2012). Since  $r_e$  is measured along a galaxy’s major axis, note that the surface-mass density here is the surface-mass density when viewed face-on, where we assume approximately circular symmetry of galaxies. The surface-mass density versus  $M_*$  is presented in Fig. 3.

We also calculate the projected central surface-mass density within 1 kpc ( $\Sigma_1$ ) for galaxies in the sample. Following Lee et al. (2018), we numerically extrapolate  $\Sigma_1$  from the best-fitting Sérsic profile in van der Wel et al. (2012):

$$I(r) = I_0 \exp \left\{ -b_n \left[ \left( \frac{r}{r_e} \right)^{1/n} - 1 \right] \right\}. \quad (4)$$

In the equation,  $I(r)$  represents light intensity at a radius of  $r$ , and  $I_0$  is the light intensity at  $r_e$ . We take the asymptotic approximation for  $b_n$  as a function of Sérsic index  $n$  following Ciotti & Bertin (1999):

$$b_n \approx 2n - \frac{1}{3} + \frac{4}{405n} + \frac{46}{2515n^2}. \quad (5)$$

Assuming a constant mass-to-light ratio throughout the galaxy, the projected central surface-mass density within 1 kpc ( $\Sigma_1$ ) can be obtained with the following equation:

$$\Sigma_1 = \frac{\int_0^{1 \text{ kpc}} I(r) 2\pi r dr}{\int_0^\infty I(r) 2\pi r dr} \frac{L_{\text{GALFIT}}}{L_{\text{phot}}} \frac{M_*}{\pi (1 \text{ kpc})^2}. \quad (6)$$

Here,  $L_{\text{phot}}$  is the total luminosity adopted from the CANDELS catalogues (Galametz et al. 2013; Guo et al. 2013; Stefanon et al. 2017; Barro et al. 2019) in the filter corresponding to the structural measurements, and  $L_{\text{GALFIT}}$  is the integrated luminosity from GALFIT. The  $L_{\text{GALFIT}}/L_{\text{phot}}$  correction term is applied following Section 3.1 of van Dokkum et al. (2014), with a median value of 1.11 and a scatter of 0.09 for objects in our sample. We note that the projected  $\Sigma_1$  values are calculated assuming galaxies follow

the measured Sérsic profiles in the central 1 kpc region. This measurement of central mass density has its limitations, since the light profiles of some galaxies in the central 1 kpc deviate from the global Sérsic profile. Utilizing the galaxy cut-outs, models, and fitting residuals provided along with van der Wel et al. (2012), we found that only  $\approx 2\%$  of galaxies in our sample have total fitting residuals in the central 1 kpc region greater than 20 % of the enclosed flux within 1 kpc. Thus, our use of the projected  $\Sigma_1$  values should be acceptable generally given the fairly mild deviations from the global Sérsic profiles in the central 1 kpc regions of galaxies. We also verified that the analysis results in Section 3 do not change qualitatively when excluding the  $\approx 2\%$  of galaxies with  $\geq 20\%$  deviations.

The projected central stellar density within 1 kpc versus mass for galaxies is presented in Fig. 4. In general, our projected  $\Sigma_1$  values are similar to those of Barro et al. (2017), who measured  $\Sigma_1$  values from stellar-mass profiles computed by fitting multiband SEDs derived from surface-brightness profiles in *HST* bands, with a systematic offset of  $\approx 0.1$  dex and a scatter of  $\approx 0.3$  dex. This agreement further indicates that our assumption of a constant mass-to-light ratio roughly holds.<sup>5</sup> In addition, unlike the measured  $\Sigma_1$  values, our projected  $\Sigma_1$  values are relatively robust against possible AGN contamination since they are extrapolated from global Sérsic profiles (although our  $\Sigma_1$  values for X-ray AGNs are also similar

<sup>5</sup>A caveat here is that SF galaxies may not follow this assumption as well as quiescent galaxies, as expected from their star formation activity. For quiescent galaxies in our sample, the systematic offset of  $\Sigma_1$  values compared with Barro et al. (2017) is  $\approx 0.0$  dex, and the scatter is  $\approx 0.1$  dex; for SF galaxies in our sample, the systematic offset is  $\approx 0.2$  dex, and the scatter is  $\approx 0.3$  dex. Also, as expected from the presence of pseudo-bulges in the Non-BD sample, SF Non-BD galaxies may not follow this assumption as well as SF BD galaxies: for galaxies in the SF BD sample, the systematic offset is  $\approx 0.0$  dex, and the scatter is  $\approx 0.2$  dex; for galaxies in the SF Non-BD sample, the systematic offset is  $\approx 0.2$  dex, and the scatter is  $\approx 0.3$  dex. Even still, these systematic offsets and scatters are acceptable since all analyses in this paper are performed based on sample-averaged values in relatively broad bins.

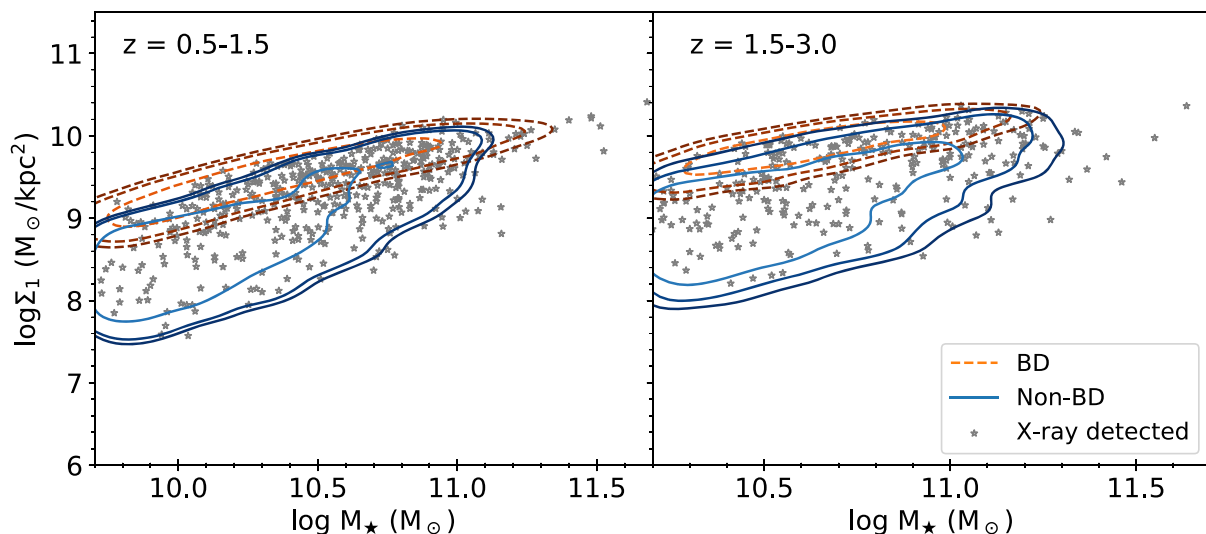


**Figure 4.** Projected central surface-mass density within 1 kpc ( $\Sigma_1$ ) versus stellar mass for galaxies in the low-redshift bin (left) and the high-redshift bin (right). The orange dashed contours encircle 68%, 90%, and 95 % of galaxies in the BD sample, and the blue solid contours encircle 68%, 90%, and 95 % of galaxies in the Non-BD sample. The grey stars mark the X-ray detected sources. Galaxies in the BD sample generally have higher  $\Sigma_1$  than galaxies in the Non-BD sample.

to those of Barro et al. 2017). We also define the central mass concentration parameter within 1 kpc ( $C_1$ )<sup>6</sup> which is independent of  $M_*$ :

$$C_1 = \frac{\int_0^{1 \text{ kpc}} I(r) 2\pi r dr}{\int_0^\infty I(r) 2\pi r dr}. \quad (7)$$

The uncertainties in  $\Sigma_1$  and  $C_1$  are propagated from the uncertainties of  $n$  and  $r_e$ . van der Wel et al. (2012) state that reliable measurements of basic size and shape parameters should be reached down to  $H = 24.5$ . For each object in the sample, we quantify the uncertainty of  $C_1$  through computing 1000  $C_1$  values from  $r_e$  values and  $n$  values with random offsets. The offsets of  $r_e$  are randomly drawn from the Gaussian distribution that has the  $1\sigma$  measurement error of  $r_e$  as the standard deviation; the offsets of  $n$  are coupled with the random offsets generated for  $r_e$ , as the errors of  $r_e$  and  $n$  are strongly correlated. The relation between  $r_e$  errors and  $n$  errors is adopted from section 2.4 of Whitaker et al. (2017). We note that even for galaxies with  $H \sim 24$ – $24.5$ , the median uncertainty of  $\log C_1$  is  $\approx 10\%$ . However, van der Wel et al. (2012) also suggest that  $n$  could only reach the accuracy of  $r_e$  among galaxies with  $H \sim 24.5$  when measured at  $H \sim 23.5$ . To assess this potential bias, we confirm that our results in Section 3 do not change when limiting the analyses to  $H < 23.5$  objects in the sample.

In Fig. 5, we show some random  $J/H$ -band cut-outs for galaxies at  $z = 0.5$ – $1.5/1.5$ – $3$ , with their properties (including redshift, morphology,  $M_*$ ,  $\Sigma_e$ ,  $\Sigma_1$ , and SFR) listed.

### 3 ANALYSES AND RESULTS

In this section, we use the analysis methods described in Section 3.1 to study how BH growth relates to host-galaxy compactness, represented by  $\Sigma_e$  (in Section 3.2) or  $\Sigma_1$  (in Section 3.3), when controlling for SFR or  $M_*$ . While  $\Sigma_e$  and  $\Sigma_1$  have both been used to

represent the compactness of galaxies,  $\Sigma_e$  measures the mass-to-size ratio in the central 50 % of galaxies, and  $\Sigma_1$  measures the mass-to-size ratio in the central 1 kpc of galaxies (see Section 2.4.3). Thus, testing how BH growth relates to both  $\Sigma_e$  and  $\Sigma_1$  when controlling for SFR or  $M_*$  can not only reveal if BH growth links with host-galaxy compactness fundamentally, but also if BH growth links more fundamentally with the compactness of the central 1 kpc regions of galaxies than the central 50 % regions of galaxies.

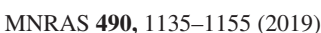
#### 3.1 Analysis methods

Yang et al. (2019) show that for bulge-dominated galaxies,  $\overline{\text{BHAR}}$  correlates with SFR when controlling for  $M_*$ , while the converse does not hold true. They also show that for galaxies that are not dominated by bulges,  $\overline{\text{BHAR}}$  correlates with  $M_*$  when controlling for SFR, while the converse does not hold true. Thus, for the BD sample, we will study whether  $\overline{\text{BHAR}}$  is mainly related to SFR or  $\Sigma$  (see Sections 3.2.1/3.3.1). We will also confine the study to SF BD galaxies only in Sections 3.2.1 and 3.3.1. For galaxies in the Non-BD sample, we will study whether  $\overline{\text{BHAR}}$  is mainly related to  $M_*$  or  $\Sigma$  (see Sections 3.2.2/3.3.2). Similarly, we will also confine the study to SF Non-BD galaxies only in Sections 3.2.2 and 3.3.2. The motivation for confining analyses to SF galaxies only is that compactness may serve as an indicator of the amount of gas in the centres of galaxies when we know that there is cold gas available, and simulations predict that BH accretion is linked with the central gas density (e.g. Wellons et al. 2015; Habouzit et al. 2019). Otherwise, if galaxies become quiescent, it is unlikely that compactness will indicate the central gas density.

For galaxies in the BD or SF BD (Non-BD or SF Non-BD) samples, we will first divide them into SFR ( $M_*$ ) bins with approximately the same number of sources per bin. We will also divide each SFR ( $M_*$ ) bin into two subsamples based on  $\Sigma$ .  $\overline{\text{BHAR}}$  and its  $1\sigma$  confidence interval (obtained via bootstrapping) will be calculated for each bin and subsample, and presented in a plot of  $\overline{\text{BHAR}}$  as a function of SFR ( $M_*$ ). We will also check if there is a significant difference in  $\overline{\text{BHAR}}$  between subsamples

<sup>6</sup>Note that  $C_1$  is different from the concentration parameter in the ‘CAS’ definition (Conselice 2003).





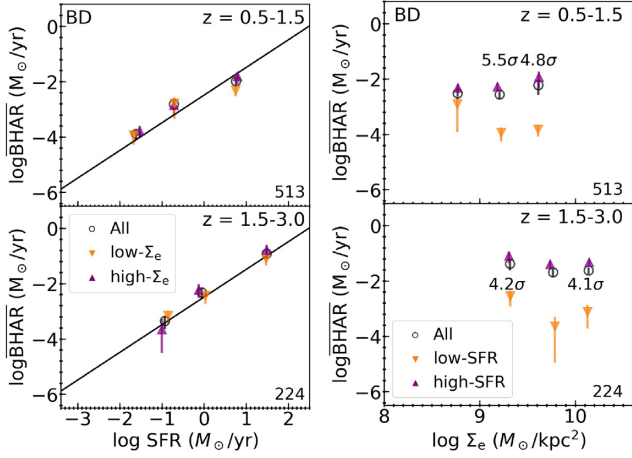


**Figure 6.**  $\overline{\text{BHAR}}$  versus SFR (left) and  $\Sigma_e$  (right) for galaxies in the BD sample. The horizontal position of each data point indicates the median SFR/ $\Sigma_e$  (left/right) of the sources in the bin. Each SFR/ $\Sigma_e$  sample (black circles) is further divided into two subsamples with  $\Sigma_e$ /SFR above (purple upward-pointing triangles) and below (orange downward-pointing triangles) the median  $\Sigma_e$ /SFR of the sample, respectively. The error bars represent the  $1\sigma$  confidence interval of  $\overline{\text{BHAR}}$  from bootstrapping. The significance levels of the differences between  $\overline{\text{BHAR}}$  in the subsamples are labelled at the position of the bin if the level is  $>3\sigma$ . The number in the bottom-right corner represents the number of objects in each SFR/ $\Sigma_e$  bin. The black solid lines in the left-hand panel represent the best-fitting  $\overline{\text{BHAR}}$ –SFR relation in Yang et al. (2019) with slope fixed to unity. We can see that while the  $\overline{\text{BHAR}}$ –SFR relation is close to that obtained in Yang et al. (2019),  $\overline{\text{BHAR}}$  does not vary with  $\Sigma_e$ .

we will utilize 6/3 bins, so each bin contains  $\approx 800/600$  ( $\approx 700/500$ ) galaxies. The relevant plots here for the BD, Non-BD, and SF Non-BD samples are Figs 6, 8, and 10, when  $\Sigma_e$  is utilized to measure compactness; Figs 12, 14, and 16 are relevant when  $\Sigma_1$  is utilized to measure compactness.

We will repeat the analyses described above with AGN fraction ( $f_{\text{AGN}}$ ; the fraction of sources with  $\log L_X > 42$ )<sup>7</sup> instead of  $\overline{\text{BHAR}}$ , which helps assess the prevalence of AGN activity instead of long-term average BH growth.  $f_{\text{AGN}}$  and its  $1\sigma$  confidence interval (also obtained via bootstrapping) will be calculated for each bin and subsample, and presented in the relevant plots. The significance level of the difference in  $f_{\text{AGN}}$  between two subsamples ( $\Delta f_{\text{AGN}} = f_{\text{AGN,subsample 1}} - f_{\text{AGN,subsample 2}}$ ) is also calculated by dividing it by its  $1\sigma$  uncertainty that is obtained from bootstrapping as (84th–16th percentile)/2 of the  $\Delta f_{\text{AGN}}$  distribution. The relevant plots here for the BD, Non-BD, and SF Non-BD samples are Figs 7, 9, and 11, when  $\Sigma_e$  is utilized to measure compactness; Figs 13, 15, and 17 are relevant, when  $\Sigma_1$  is utilized to measure compactness.

<sup>7</sup>We choose this ‘ $\log L_X > 42$ ’ criterion to select AGNs consistently with previous works, including Kocevski et al. (2017). We note that we cannot obtain a complete selection of objects with  $\log L_X > 42$  at  $z \sim 0.7$ – $3$  considering the X-ray flux detection limits of COSMOS, UDS, and EGS (Nandra et al. 2015; Civano et al. 2016; Kocevski et al. 2018). Since we mainly utilize this criterion to probe the potential difference in  $f_{\text{AGN}}$  between different samples in our study, we do not necessarily require a complete  $\log L_X > 42$  selection: if a significant difference in the fraction of objects with  $\log L_X > 42$  is observed between two samples, given that AGNs with relatively low  $L_X$  can only be detected in relatively deep X-ray fields, the intrinsic difference in AGN fraction will be more significant (unless the differences in the fraction of low- $L_X$  and high- $L_X$  AGNs have different signs).

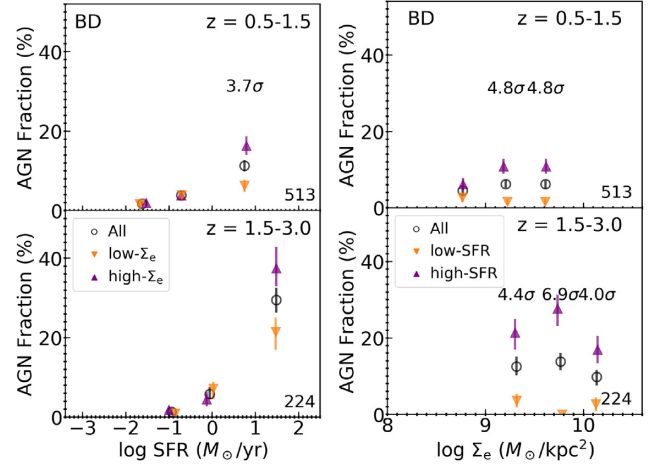


**Figure 7.** AGN fraction versus SFR (left) and  $\Sigma_e$  (right) for galaxies in the BD sample. The horizontal position of each data point indicates the median SFR/ $\Sigma_e$  (left/right) of the sources in the bin. Each SFR/ $\Sigma_e$  sample (black circles) is further divided into two subsamples with  $\Sigma_e$ /SFR above (purple upward-pointing triangles) and below (orange downward-pointing triangles) the median  $\Sigma_e$ /SFR of the sample, respectively. The error bars represent the  $1\sigma$  confidence interval of AGN fraction from bootstrapping. The significance levels of the differences between AGN fraction in the subsamples are labelled at the position of the bin if the level is  $>3\sigma$ . The number in the bottom-right corner represents the number of objects in each SFR/ $\Sigma_e$  bin. We can see that while AGN fraction varies with SFR, it does not vary significantly with  $\Sigma_e$ .

We will perform PCOR analyses with PCOR.R in the R statistical package (Kim 2015) to assess if, for galaxies in the BD (Non-BD or SF Non-BD) sample, the  $\overline{\text{BHAR}}$ –SFR relation ( $\overline{\text{BHAR}}-M_*$  relation) is still significant when controlling for  $\Sigma$ . We will also assess if the  $\overline{\text{BHAR}}-\Sigma$  relation is significant when controlling for SFR ( $M_*$ ). We will bin sources based on both SFR ( $M_*$ ) and  $\Sigma$ , and calculate  $\overline{\text{BHAR}}$  for each bin. The bins for the  $x$ -axis or  $y$ -axis are chosen to include approximately the same numbers of sources. Only bins with more than 50 objects will be utilized in the PCOR analyses to avoid large statistical uncertainties as well as potential systematic problems due to occasional ‘outlier’ objects that could perturb a small sample. Bins, where  $\overline{\text{BHAR}}$  does not have a lower limit  $> 0$  from bootstrapping, will also be excluded from the PCOR analyses. We will input the median log SFR ( $M_*$ ), median log  $\Sigma$ , and log  $\overline{\text{BHAR}}$  of utilized bins to PCOR.R, to calculate the significance levels of the  $\overline{\text{BHAR}}-\text{SFR}$  ( $\overline{\text{BHAR}}-M_*$ ) relation, when controlling for  $\Sigma$  and the  $\overline{\text{BHAR}}-\Sigma$  relation when controlling for SFR ( $M_*$ ) with both the Pearson and Spearman statistics. We will summarize the results of the PCOR analyses in tables (Table 2 when  $\Sigma_e$  is utilized, and Table 3 when  $\Sigma_1$  is utilized). We will use the parametric Pearson statistic to select significant results, and the non-parametric Spearman statistic will also be presented. Typically, the significance level obtained utilizing the Spearman statistic is qualitatively consistent with that obtained from the Pearson statistic. For the PCOR analyses at  $z = 0.5$ – $1.5/1.5$ – $3$ , we will adopt a  $3 \times 3$  grid for the BD sample, so that each bin contains  $\approx 170/70$  sources on average; we will adopt a  $5 \times 5/3 \times 3$  grid for the Non-BD (SF Non-BD) sample, so that each bin contains  $\approx 190/210$  (160/180) sources on average. As for the SF BD sample, we are not able to perform PCOR analyses due to its limited sample size. For all the PCOR analyses in this work,  $\gtrsim 98\%$  of sources in the sample are included with the utilized binning approach. When a  $5 \times 5$  grid is

**Table 2.**  $p$ -values (significances) of partial correlation analyses for the BHAR– $\Sigma_e$  relation.

Relation	Pearson	Spearman
BD: $0.5 \leq z < 1.5$ ( $3 \times 3$ bins)		
$\overline{\text{BHAR}}\text{--SFR}$	$3 \times 10^{-4}$ ( <b>3.6<math>\sigma</math></b> )	$1 \times 10^{-5}$ ( <b>4.4<math>\sigma</math></b> )
$\overline{\text{BHAR}}\text{--}\Sigma_e$	0.29 (1.1 $\sigma$ )	0.68 (0.4 $\sigma$ )
BD: $1.5 \leq z < 3$ ( $3 \times 3$ bins)		
$\overline{\text{BHAR}}\text{--SFR}$	$2 \times 10^{-3}$ ( <b>3.2<math>\sigma</math></b> )	0.01 (2.5 $\sigma$ )
$\overline{\text{BHAR}}\text{--}\Sigma_e$	0.44 (0.8 $\sigma$ )	0.28 (1.1 $\sigma$ )
Non-BD: $0.5 \leq z < 1.5$ ( $5 \times 5$ bins)		
$\overline{\text{BHAR}}\text{--}M_*$	$3 \times 10^{-3}$ ( <b>3.0<math>\sigma</math></b> )	$8 \times 10^{-4}$ ( <b>3.4<math>\sigma</math></b> )
$\overline{\text{BHAR}}\text{--}\Sigma_e$	0.42 (0.8 $\sigma$ )	0.86 (0.2 $\sigma$ )
Non-BD: $1.5 \leq z < 3$ ( $3 \times 3$ bins)		
$\overline{\text{BHAR}}\text{--}M_*$	$3 \times 10^{-3}$ ( <b>3.0<math>\sigma</math></b> )	$3 \times 10^{-3}$ ( <b>3.0<math>\sigma</math></b> )
$\overline{\text{BHAR}}\text{--}\Sigma_e$	0.40 (0.8 $\sigma$ )	0.46 (0.7 $\sigma$ )
SF Non-BD: $0.5 \leq z < 1.5$ ( $5 \times 5$ bins)		
$\overline{\text{BHAR}}\text{--}M_*$	$1 \times 10^{-3}$ ( <b>3.2<math>\sigma</math></b> )	$6 \times 10^{-3}$ (2.7 $\sigma$ )
$\overline{\text{BHAR}}\text{--}\Sigma_e$	0.13 (1.5 $\sigma$ )	0.37 (0.9 $\sigma$ )
$\overline{\text{BHAR}}\text{--}M_*$	$1 \times 10^{-8}$ ( <b>5.7<math>\sigma</math></b> )	$2 \times 10^{-7}$ ( <b>5.2<math>\sigma</math></b> )
$\overline{\text{BHAR}}\text{--}r_e$	0.08 (1.7 $\sigma$ )	0.11 (1.6 $\sigma$ )
SF Non-BD: $1.5 \leq z < 3$ ( $3 \times 3$ bins)		
$\overline{\text{BHAR}}\text{--}M_*$	0.02 (2.4 $\sigma$ )	0.02 (2.4 $\sigma$ )
$\overline{\text{BHAR}}\text{--}\Sigma_e$	0.35 (0.9 $\sigma$ )	0.93 (0.1 $\sigma$ )
$\overline{\text{BHAR}}\text{--}M_*$	$7 \times 10^{-4}$ ( <b>3.4<math>\sigma</math></b> )	$1 \times 10^{-3}$ ( <b>3.2<math>\sigma</math></b> )
$\overline{\text{BHAR}}\text{--}r_e$	0.48 (0.7 $\sigma$ )	0.36 (0.9 $\sigma$ )

adopted, we will also perform tests with a  $3 \times 3$  grid and a  $4 \times 4$  grid. Typically, our results do not change qualitatively with the choice of grid; we will note in the text if a result is only significant with a  $5 \times 5$  grid. We have also verified that our results do not change qualitatively with different binning approaches, e.g. binning based on equal intervals for the  $x$ -axis or  $y$ -axis, or binning on one axis first and then another axis to make each bin have approximately the same number of sources.

### 3.2 The relation between BH growth and $\Sigma_e$

In this section, we study how BH growth relates to  $\Sigma_e$  (which measures host-galaxy compactness more globally compared with  $\Sigma_1$ ; see Section 2.4.3) when controlling for SFR or  $M_*$  among galaxies in the BD sample (see Section 3.2.1) and Non-BD sample (see Section 3.2.2), respectively. Figs 6–11 are relevant for this subsection, and note we use a consistent black–purple–orange colour scheme for these figures.

#### 3.2.1 How does BH growth relate to $\Sigma_e$ for bulge-dominated galaxies?

We plot  $\overline{\text{BHAR}}$  as a function of SFR and  $\Sigma_e$  in Fig. 6 for galaxies in the BD sample. Each SFR/ $\Sigma_e$  bin is further divided into two subsamples with  $\Sigma_e$ /SFR above or below the median  $\Sigma_e$ /SFR, and the  $\overline{\text{BHAR}}$  values of these subsamples are shown on the plot as well. We can see that for galaxies in the BD sample, there is no obvious  $\overline{\text{BHAR}}\text{--}\Sigma_e$  relation (in the right-hand panel of Fig. 6), and for a given SFR, the differences in  $\Sigma_e$  do not cause any significant differences in  $\overline{\text{BHAR}}$  (in the left-hand panel of Fig. 6). This qualitatively indicates

**Table 3.**  $p$ -values (significances) of partial correlation analyses for the BHAR– $\Sigma_1$  relation.

Relation	Pearson	Spearman
BD: $0.5 \leq z < 1.5$ ( $3 \times 3$ bins)		
$\overline{\text{BHAR}}\text{--SFR}$	$2 \times 10^{-3}$ ( <b>3.1<math>\sigma</math></b> )	$3 \times 10^{-4}$ ( <b>3.6<math>\sigma</math></b> )
$\overline{\text{BHAR}}\text{--}\Sigma_1$	0.19 (1.3 $\sigma$ )	0.69 (0.4 $\sigma$ )
$\overline{\text{BHAR}}\text{--SFR}$	$1 \times 10^{-3}$ ( <b>3.3<math>\sigma</math></b> )	$2 \times 10^{-4}$ ( <b>3.7<math>\sigma</math></b> )
$\overline{\text{BHAR}}\text{--}C_1$	0.56 (0.6 $\sigma$ )	0.44 (0.8 $\sigma$ )
BD: $1.5 \leq z < 3$ ( $3 \times 3$ bins)		
$\overline{\text{BHAR}}\text{--SFR}$	$5 \times 10^{-4}$ ( <b>3.5<math>\sigma</math></b> )	$1 \times 10^{-3}$ ( <b>3.2<math>\sigma</math></b> )
$\overline{\text{BHAR}}\text{--}\Sigma_1$	0.23 (1.2 $\sigma$ )	0.86 (0.2 $\sigma$ )
$\overline{\text{BHAR}}\text{--SFR}$	$2 \times 10^{-4}$ ( <b>3.8<math>\sigma</math></b> )	$2 \times 10^{-3}$ ( <b>3.1<math>\sigma</math></b> )
$\overline{\text{BHAR}}\text{--}C_1$	0.70 (0.4 $\sigma$ )	0.17 (1.4 $\sigma$ )
Non-BD: $0.5 \leq z < 1.5$ ( $5 \times 5$ bins)		
$\overline{\text{BHAR}}\text{--}M_*$	0.03 (2.2 $\sigma$ )	0.16 (1.4 $\sigma$ )
$\overline{\text{BHAR}}\text{--}\Sigma_1$	$4 \times 10^{-3}$ (2.9 $\sigma$ )	0.02 (2.4 $\sigma$ )
$\overline{\text{BHAR}}\text{--}M_*$	$8 \times 10^{-8}$ ( <b>5.4<math>\sigma</math></b> )	$2 \times 10^{-7}$ ( <b>5.2<math>\sigma</math></b> )
$\overline{\text{BHAR}}\text{--}C_1$	0.01 (2.6 $\sigma$ )	0.02 (2.3 $\sigma$ )
Non-BD: $1.5 \leq z < 3$ ( $3 \times 3$ bins)		
$\overline{\text{BHAR}}\text{--}M_*$	0.06 (1.9 $\sigma$ )	0.36 (0.9 $\sigma$ )
$\overline{\text{BHAR}}\text{--}\Sigma_1$	0.11 (1.6 $\sigma$ )	0.27 (1.1 $\sigma$ )
$\overline{\text{BHAR}}\text{--}M_*$	$2 \times 10^{-3}$ ( <b>3.1<math>\sigma</math></b> )	$4 \times 10^{-4}$ ( <b>3.5<math>\sigma</math></b> )
$\overline{\text{BHAR}}\text{--}C_1$	0.08 (1.8 $\sigma$ )	0.03 (2.1 $\sigma$ )
SF Non-BD: $0.5 \leq z < 1.5$ ( $5 \times 5$ bins)		
$\overline{\text{BHAR}}\text{--}M_*$	0.02 (2.3 $\sigma$ )	0.01 (2.4 $\sigma$ )
$\overline{\text{BHAR}}\text{--}\Sigma_1$	0.01 (2.5 $\sigma$ )	0.11 (1.6 $\sigma$ )
$\overline{\text{BHAR}}\text{--}M_*$	$4 \times 10^{-6}$ ( <b>4.6<math>\sigma</math></b> )	$2 \times 10^{-6}$ ( <b>4.8<math>\sigma</math></b> )
$\overline{\text{BHAR}}\text{--}C_1$	$3 \times 10^{-3}$ ( <b>3.0<math>\sigma</math></b> )	$3 \times 10^{-3}$ ( <b>3.0<math>\sigma</math></b> )
SF Non-BD: $1.5 \leq z < 3$ ( $3 \times 3$ bins)		
$\overline{\text{BHAR}}\text{--}M_*$	0.03 (2.2 $\sigma$ )	0.05 (2.0 $\sigma$ )
$\overline{\text{BHAR}}\text{--}\Sigma_1$	0.21 (1.3 $\sigma$ )	0.92 (0.1 $\sigma$ )
$\overline{\text{BHAR}}\text{--}M_*$	$4 \times 10^{-3}$ (2.9 $\sigma$ )	$2 \times 10^{-3}$ ( <b>3.2<math>\sigma</math></b> )
$\overline{\text{BHAR}}\text{--}C_1$	0.29 (1.1 $\sigma$ )	0.56 (0.6 $\sigma$ )

that  $\overline{\text{BHAR}}$  does not depend on  $\Sigma_e$ . Given that we define high- or low- $\Sigma_e$  subsamples based on median  $\Sigma_e$  values, it is possible that the difference in  $\overline{\text{BHAR}}$  associated with  $\Sigma_e$  might only be revealed by subsamples of extreme  $\Sigma_e$ . Considering this, we confirm that even when defining  $\Delta\overline{\text{BHAR}}$  as the difference between  $\overline{\text{BHAR}}$  of a subsample of galaxies with  $\Sigma_e$  greater than the 75th percentile of the  $\Sigma_e$  distribution and a subsample of galaxies with  $\Sigma_e$  less than the 25th percentile of the  $\Sigma_e$  distribution, we do not observe significant  $\Delta\overline{\text{BHAR}}$  associated with  $\Sigma_e$ . To test the point that BHAR does not depend on  $\Sigma_e$  in the BD sample further, we bin sources based on both SFR and  $\Sigma_e$  (with the binning approach described in Section 3.1), and use the median log SFR, median log  $\Sigma_e$ , and log  $\overline{\text{BHAR}}$  of bins to perform PCOR analyses. The results are summarized in Table 2. While the  $\overline{\text{BHAR}}\text{--SFR}$  relation is significant as expected when controlling for  $\Sigma_e$ ,  $\overline{\text{BHAR}}$  does not correlate with  $\Sigma_e$  significantly when controlling for SFR in the BD sample.

We also investigate how AGN fraction relates to  $\Sigma_e$  when controlling for SFR for the BD sample. In Fig. 7, we plot AGN fraction as a function of SFR and  $\Sigma_e$  for galaxies in the BD sample. The bins and subsamples in Fig. 7 are the same as those of Fig. 6.



We can see that while AGN fraction does not vary significantly with  $\Sigma_e$  (in the right-hand panel of Fig. 7), it rises at the high-SFR end (in the left-hand panel of Fig. 7). Also, the  $f_{\text{AGN}}$  differences associated with  $\Sigma_e$  when controlling for SFR are not significant except for one bin with the highest SFR at  $z = 0.5-1.5$ , as can be seen in the left-hand panel of Fig. 7. If we consider the Bonferroni correction to counteract the problem of multiple comparisons (see Section 1; since we are testing six hypotheses together here, we require the difference to be significant at  $>3.5\sigma$ ), this  $3.7\sigma$  difference is still significant.

Could this suggest a dependence of AGN fraction on  $\Sigma_e$  among SF galaxies in the BD sample? Due to the limited number of SF BD galaxies, we calculate the significance level of  $\Delta f_{\text{AGN}}$  for all SF BD galaxies at  $z = 0.5-1.5/1.5-3$  when splitting into high- or low- $\Sigma_e$  subsamples, which is  $3.7\sigma/2.6\sigma$ . In terms of  $\Delta \text{BHAR}$ , the significance levels at both  $z = 0.5-1.5$  and  $z = 1.5-3$  are below  $3\sigma$ . We also note that when splitting all SF BD galaxies into high- or low- $M_*$  subsamples, the significance level of  $\Delta f_{\text{AGN}}$  is  $6.3\sigma/2.5\sigma$  at  $z = 0.5-1.5/1.5-3$ , and the significance level of  $\Delta \text{BHAR}$  is  $6.4\sigma/3.7\sigma$ . Interestingly, when splitting all SF BD galaxies into high- or low-SFR subsamples, the  $\Delta \text{BHAR}/\Delta f_{\text{AGN}}$  between two subsamples in both redshift ranges are not significant. As mentioned in Section 3.1, the sample size of SF BD galaxies is too small to perform PCOR analyses to disentangle the relative roles of  $M_*$  and  $\Sigma_e$  effects. However, we note that the influence of  $M_*$  is more significant than the influence of  $\Sigma_e$  in both  $\text{BHAR}$  and  $f_{\text{AGN}}$ .

Thus, for galaxies in the BD sample,  $\Sigma_e$  has no apparent relation to either the long-term average BH growth or the prevalence of AGN activity.

### 3.2.2 How does BH growth relate to $\Sigma_e$ for galaxies that are not bulge-dominated?

In Fig. 8, we plot  $\text{BHAR}$  as a function of  $M_*$  and  $\Sigma_e$  for the Non-BD sample. Each  $M_*/\Sigma_e$  bin is further divided into two subsamples with  $\Sigma_e/M_*$  above or below the median  $\Sigma_e/M_*$ , and the BHAR values of these subsamples are shown on the plot as well. We can see that while both the  $\text{BHAR}-M_*$  relation and  $\text{BHAR}-\Sigma_e$  relation exist with non-zero slope (which is expected given the degeneracy between  $M_*$  and  $\Sigma_e$  in Fig. 3), in most cases the differences in  $M_*$  for a given  $\Sigma_e$  (in the right-hand panel) are linked with noticeable differences in BHAR, and the differences in  $\Sigma_e$  for a given  $M_*$  (in the left-hand panel) do not lead to significant differences in BHAR. We confirm that even when defining  $\Delta \text{BHAR}$  as the difference between  $\text{BHAR}$  of a subsample of galaxies with  $\Sigma_e$  greater than the 75th percentile of the  $\Sigma_e$  distribution and a subsample of galaxies with  $\Sigma_e$  less than the 25th percentile of the  $\Sigma_e$  distribution, we do not observe significant  $\Delta \text{BHAR}$  linked with  $\Sigma_e$ .

We then perform PCOR analyses to test quantitatively if the  $\text{BHAR}-\Sigma_e$  relation is a secondary manifestation of the  $\text{BHAR}-M_*$  relation. We bin sources based on both  $M_*$  and  $\Sigma_e$  and calculate  $\text{BHAR}$  for each bin. The median  $\log M_*$ , median  $\log \Sigma_e$ , and  $\log \text{BHAR}$  of these bins are used for PCOR analyses to calculate the significance levels of the  $\text{BHAR}-M_*$  relation when controlling for  $\Sigma_e$  and the  $\text{BHAR}-\Sigma_e$  relation when controlling for  $M_*$ . The results are summarized in Table 2. We can see that while  $\text{BHAR}$  significantly depends on  $M_*$  as expected when controlling for  $\Sigma_e$ ,  $\text{BHAR}$  does not correlate significantly with  $\Sigma_e$  when controlling for  $M_*$ . Thus, the  $\text{BHAR}-\Sigma_e$  relation among galaxies in the Non-BD sample is not fundamental.

We also investigate how the prevalence of AGN relates to

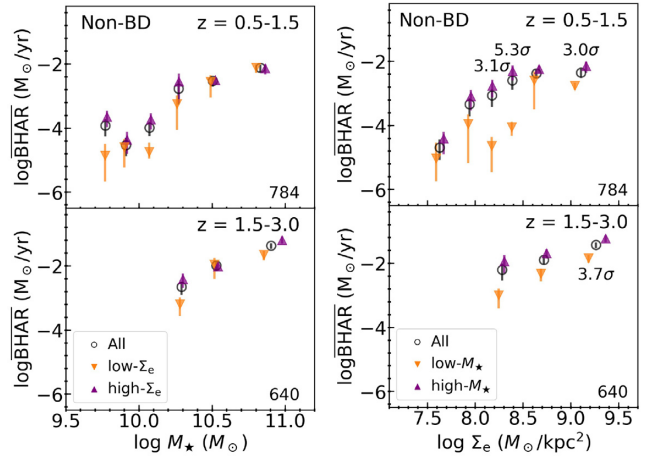


**Figure 8.**  $\text{BHAR}$  versus  $M_*$  (left) and  $\Sigma_e$  (right) for galaxies in the Non-BD sample. The horizontal position of each data point indicates the median  $M_*/\Sigma_e$  (left/right) of the sources in the bin. Each  $M_*/\Sigma_e$  sample (black circles) is further divided into two subsamples with  $\Sigma_e/M_*$  above (purple upward-pointing triangles) and below (orange downward-pointing triangles) the median  $\Sigma_e/M_*$  of the sample, respectively. The error bars represent the  $1\sigma$  confidence interval of BHAR from bootstrapping. The significance levels of the differences between  $\text{BHAR}$  in the subsamples are labelled at the position of the bin if the level is  $>3\sigma$ . The number in the bottom-right corner represents the number of objects in each  $M_*/\Sigma_e$  bin. While we can see both the  $\text{BHAR}-M_*$  and  $\text{BHAR}-\Sigma_e$  relations,  $\Delta \text{BHAR}$  values associated with  $M_*$  are generally noticeable (in the right-hand panel) and all  $\Delta \text{BHAR}$  values associated with  $\Sigma_e$  are not significant (in the left-hand panel).

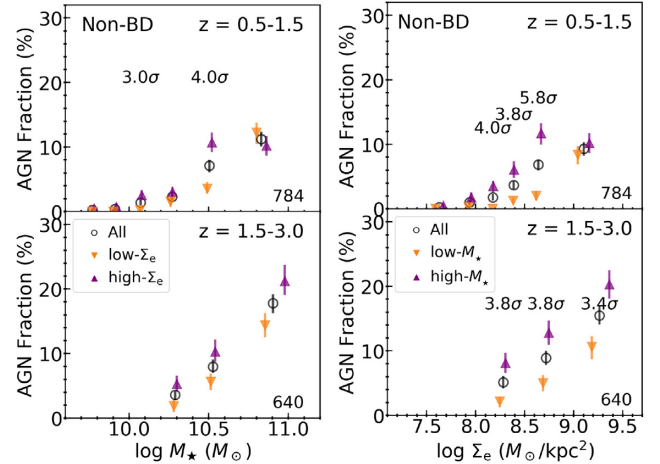


**Figure 9.** AGN fraction versus  $M_*$  (left) and  $\Sigma_e$  (right) for galaxies in the Non-BD sample. The horizontal position of each data point indicates the median  $M_*/\Sigma_e$  (left or right) of the sources in the bin. Each  $M_*/\Sigma_e$  sample (black circles) is further divided into two subsamples with  $\Sigma_e/M_*$  above (purple upward-pointing triangles) and below (orange downward-pointing triangles) the median  $\Sigma_e/M_*$  of the sample, respectively. The error bars represent the  $1\sigma$  confidence interval of AGN fraction from bootstrapping. The significance levels of the differences between AGN fraction in the subsamples are labelled at the position of the bin if the level is  $>3\sigma$ . The number in the bottom-right corner represents the number of objects in each  $M_*/\Sigma_e$  bin. We can see that  $\Delta f_{\text{AGN}}$  values associated with  $M_*$  are generally noticeable (in the right-hand panel), and almost all  $\Delta f_{\text{AGN}}$  values associated with  $\Sigma_e$  are not significant (in the left-hand panel) considering the Bonferroni correction except for one bin with  $\log M_* \approx 10.5$  at  $z = 0.5-1.5$ .

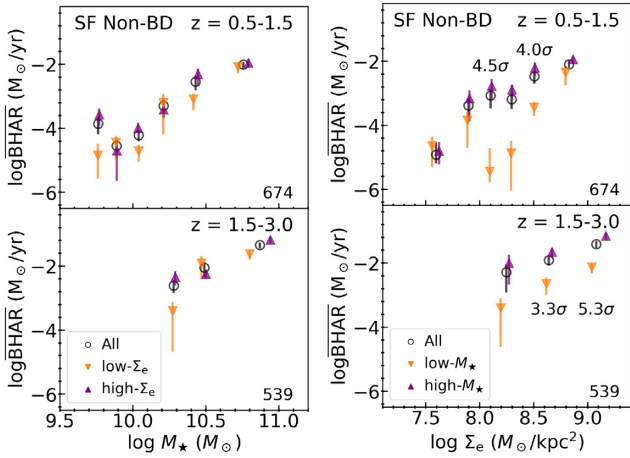


**Figure 10.** Similar to Fig. 8, but for galaxies in the SF Non-BD sample.  $\Delta\text{BHAR}$  values associated with  $M_*$  are generally noticeable (in the right-hand panel) and all  $\Delta\text{BHAR}$  values associated with  $\Sigma_e$  are not significant (in the left-hand panel).

$\Sigma_e$  when controlling for  $M_*$  for the Non-BD sample. In Fig. 9, we plot AGN fraction as a function of  $M_*$  and  $\Sigma_e$  for galaxies in the Non-BD sample. The bins and subsamples in Fig. 9 are the same as those of Fig. 8. We can see that, similar to the case for  $\text{BHAR}$ , the differences in  $M_*$  for a given  $\Sigma_e$  (in the right-hand panel) are generally linked with noticeable differences in AGN fraction, and the differences in  $\Sigma_e$  for a given  $M_*$  (in the left-hand panel) are not. Interestingly, for one bin with median  $\log M_* \approx 10.5$  at  $z = 0.5-1.5$ ,  $\Delta f_{\text{AGN}}$  has a significance level of  $4.0\sigma$ . Even when the Bonferroni correction is considered (since we are testing nine hypotheses together here, we require the difference to be significant at  $>3.6\sigma$ ), this difference is still significant. However, as can be seen in Fig. 8, the  $\Delta\text{BHAR}$  for this bin is not significant ( $0.2\sigma$ ). We find that the difference in AGN fraction here is mainly a result of a higher fraction of low- $L_X$  AGN ( $L_X = 10^{42-43} \text{ erg s}^{-1}$ ) among high- $\Sigma_e$  galaxies than low- $\Sigma_e$  galaxies in this mass range. At the same time, the fraction of high- $L_X$  AGN ( $L_X > 10^{43} \text{ erg s}^{-1}$ ) does not significantly vary with  $\Sigma_e$  in this mass range, leading to the lack of difference in BHAR. We note that this difference in AGN fraction linked with  $\Sigma_e$  when  $\log M_* \approx 10.5$  at  $z = 0.5-1.5$  is not caused by any potential dependence of AGN fraction on SFR: for this  $M_*$  bin, the difference in AGN fraction linked with SFR is not significant ( $0\sigma$ ). We will discuss the possible reason for this significant  $\Delta f_{\text{AGN}}$  associated with  $\Sigma_e$  that only occurs within certain mass ranges in Section 4.1.2.

We also confined the objects under investigation to be only SF galaxies in the Non-BD sample to study the relation between BH growth and  $\Sigma_e$ , where  $\Sigma_e$  may serve as an indicator of the gas density within  $r_e$ . The  $\text{BHAR}/f_{\text{AGN}}$  as a function of  $M_*/\Sigma_e$  among SF Non-BD galaxies is presented in Figs 10 and 11. Similar to the results for galaxies in the Non-BD sample, a  $\Delta\text{BHAR}$  link with  $\Sigma_e$  is not significant in any  $M_*$  bin. A  $\Delta f_{\text{AGN}}$  link with  $\Sigma_e$  is only significant (at  $3.7\sigma$ ) for one bin with median  $\log M_* \approx 10.4$  at  $z = 0.5-1.5$ . This mass range is similar to that of the  $M_*$  bin where a  $4.0\sigma$   $\Delta f_{\text{AGN}}$  associated with  $\Sigma_e$  is observed for the Non-BD sample at  $z = 0.5-1.5$ . The significance levels of the  $\text{BHAR}-M_*$  relation and the  $\text{BHAR}-\Sigma_e$  relation obtained from PCOR analyses for galaxies in the SF Non-BD sample are summarized in Table 2: the  $\text{BHAR}-\Sigma_e$  relation is not significant when controlling for  $M_*$ . However, the  $\text{BHAR}-M_*$  relation is also not always significant (though it is

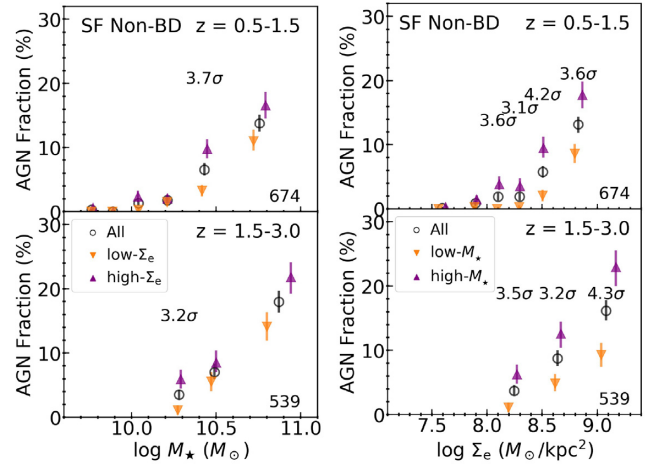


**Figure 11.** Similar to Fig. 9, but for galaxies in the SF Non-BD sample. We can see that  $\Delta f_{\text{AGN}}$  values associated with  $M_*$  are generally noticeable (in the right-hand panel), and almost all  $\Delta f_{\text{AGN}}$  values associated with  $\Sigma_e$  are not significant (in the left-hand panel) considering the Bonferroni correction (significant if  $>3.6\sigma$  when 9 hypotheses are tested together) except for one bin with  $\log M_* \approx 10.4$  at  $z = 0.5-1.5$ . The bin with  $\log M_* \approx 10.3$  at  $z = 1.5-3$  also has nearly significant  $\Delta f_{\text{AGN}}$  associated with  $\Sigma_e$ .

still more significant than the  $\text{BHAR}-\Sigma_e$  relation), probably due to the degeneracy between  $M_*$  and  $\Sigma_e$  among SF galaxies (e.g. see fig. 2 of Barro et al. 2017). Thus, for galaxies in the SF Non-BD sample, we further test if the  $\text{BHAR}-r_e$  relation is significant when controlling for  $M_*$ , which can reveal if  $\text{BHAR}$  truly depends on  $\Sigma_e$ , as  $\log \Sigma_e = \log M_* - 2 \times \log r_e + \text{Constant}$  from the definition  $\Sigma_e = 0.5M_*/\pi r_e^2$ . The results are also summarized in Table 2. We find that the  $\text{BHAR}-r_e$  relation is not significant when controlling for  $M_*$ , suggesting that the  $\text{BHAR}-\Sigma_e$  relation is also not fundamental among SF Non-BD galaxies. We note that previous studies found significantly elevated BH growth among high- $\Sigma_e$  galaxies compared with low- $\Sigma_e$  galaxies, and we will explain how this result compares with our findings in Section 4.1.1.

### 3.3 The relation between BH growth and $\Sigma_1$

In this section, we perform the same analyses as those in Section 3.2, but now utilizing the projected central surface-mass density,  $\Sigma_1$ , to represent the host-galaxy compactness. As noted in Section 1,  $\Sigma_1$  has the potential of being a more effective indicator of BH growth compared with  $\Sigma_e$ . Thus, we will test if BH growth indeed has a fundamental dependence on host-galaxy compactness that can only be effectively revealed by  $\Sigma_1$ , given the failure to find a fundamental  $\text{BHAR}-\Sigma_e$  relation in Section 3.2. Figs 12–18 are relevant for this subsection, and note we use a consistent black–blue–red colour scheme for these figures.

#### 3.3.1 How does BH growth relate to $\Sigma_1$ for the bulge-dominated galaxies?

We plot  $\text{BHAR}$  as a function of SFR and  $\Sigma_1$  in Fig. 12 for galaxies in the BD sample. Each SFR/ $\Sigma_1$  bin is further divided into two subsamples with  $\Sigma_1/\text{SFR}$  above or below the median  $\Sigma_1/\text{SFR}$ , and the  $\text{BHAR}$  values of these subsamples are shown on the plot as well. Similarly, we plot  $f_{\text{AGN}}$  as a function of SFR and  $\Sigma_1$  in Fig. 13. The bins and subsamples of Fig. 13 are the same as those of Fig. 12. We can see that for all galaxies in the BD sample, there is no obvious

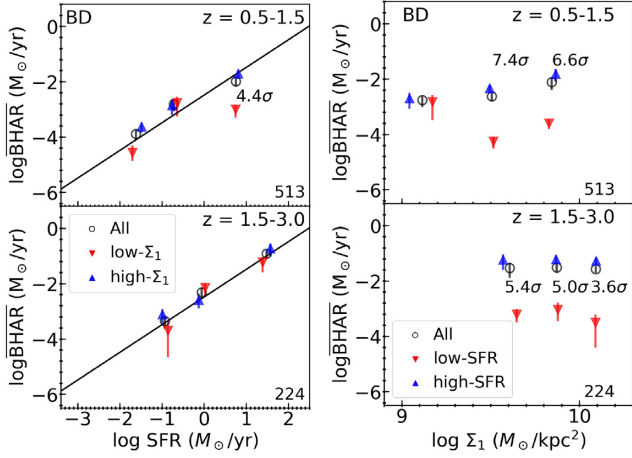


**Figure 12.**  $\overline{\text{BHAR}}$  versus SFR (left) and  $\Sigma_1$  (right) for galaxies in the BD sample. The horizontal position of each data point indicates the median SFR/ $\Sigma_1$  (left/right) of the sources in the bin. Each SFR/ $\Sigma_1$  sample (black circles) is further divided into two subsamples with  $\Sigma_1$ /SFR above (blue upward-pointing triangles) and below (red downward-pointing triangles) the median  $\Sigma_1$ /SFR of the sample, respectively. The error bars represent the  $1\sigma$  confidence interval of  $\overline{\text{BHAR}}$  from bootstrapping. The significance levels of the differences between  $\overline{\text{BHAR}}$  in the subsamples are labelled at the position of the bin if the level is  $>3\sigma$ . The number in the bottom-right corner represents the number of objects in each SFR/ $\Sigma_1$  bin. The black solid lines in the left-hand panel represent the best-fitting  $\overline{\text{BHAR}}$ –SFR relation in Yang et al. (2019) with slope fixed to unity. We can see that  $\overline{\text{BHAR}}$  does not vary substantially with  $\Sigma_1$ .

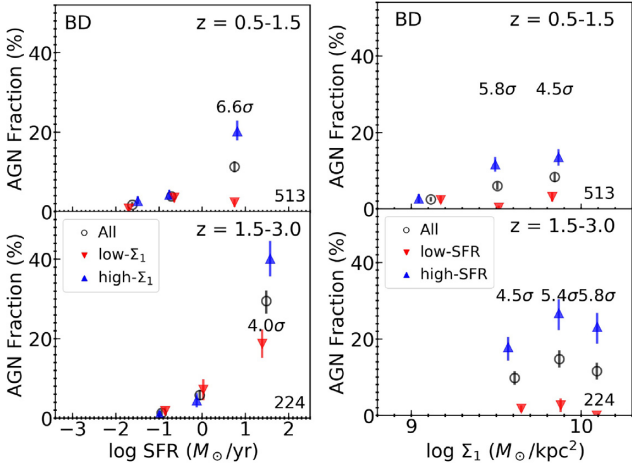


**Figure 13.** AGN fraction versus SFR (left) and  $\Sigma_1$  (right) for galaxies in the BD sample. The horizontal position of each data point indicates the median SFR/ $\Sigma_1$  (left/right) of the sources in the bin. Each SFR/ $\Sigma_1$  sample (black circles) is further divided into two subsamples with  $\Sigma_1$ /SFR above (blue upward-pointing triangles) and below (red downward-pointing triangles) the median  $\Sigma_1$ /SFR of the sample, respectively. The error bars represent the  $1\sigma$  confidence interval of AGN fraction from bootstrapping. The significance levels of the differences between AGN fraction in the subsamples are labelled at the position of the bin if the level is  $>3\sigma$ . The number in the bottom-right corner represents the number of objects in each SFR/ $\Sigma_1$  bin. We can see that the differences in  $\Sigma_1$  do not cause significant differences in  $f_{\text{AGN}}$  except for the highest SFR bin at both redshift ranges.

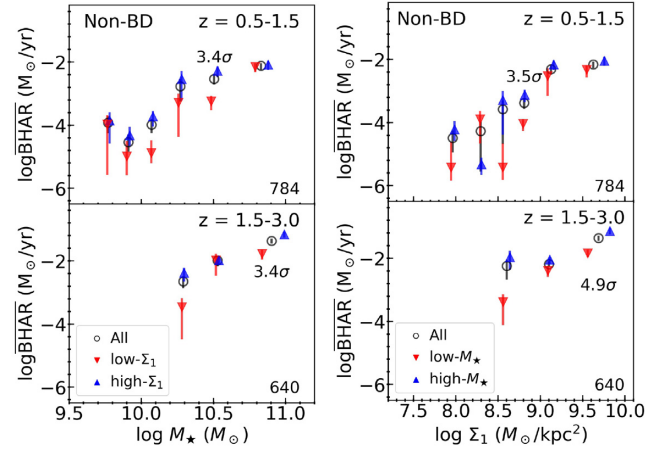


**Figure 14.**  $\overline{\text{BHAR}}$  versus  $M_*$  (left) and  $\Sigma_1$  (right) for galaxies in the Non-BD sample. The horizontal position of each data point indicates the median  $M_*/\Sigma_1$  (left/right) of the sources in the bin. Each  $M_*/\Sigma_1$  sample (black circles) is further divided into two subsamples with  $\Sigma_1/M_*$  above (blue upward-pointing triangles) and below (red downward-pointing triangles) the median  $\Sigma_1/M_*$  of the sample, respectively. The error bars represent the  $1\sigma$  confidence interval of  $\overline{\text{BHAR}}$  from bootstrapping. The significance levels of the differences between  $\overline{\text{BHAR}}$  in the subsamples are labelled at the position of the bin if the level is  $>3\sigma$ . The number in the bottom-right corner represents the number of objects in each  $M_*/\Sigma_1$  bin. Noticeable  $\Delta\overline{\text{BHAR}}$  values are associated with both  $M_*$  and  $\Sigma_1$ .

$\overline{\text{BHAR}}$ – $\Sigma_1$  relation (in the right-hand panel of Fig. 12). For a given SFR, the differences in  $\Sigma_1$  do not cause significant differences in  $\overline{\text{BHAR}}$  except for the highest SFR bin at  $z = 0.5$ – $1.5$  (in the left-hand panel of Fig. 12), and do not cause significant differences in  $f_{\text{AGN}}$  except for the highest SFR bin at both  $z = 0.5$ – $1.5$  and  $z = 1.5$ – $3$  (in the left-hand panel of Fig. 13).

We thus confine our attention to SF BD galaxies, and calculate the significance level of  $\Delta\overline{\text{BHAR}}$  ( $\Delta f_{\text{AGN}}$ ) for all SF BD galaxies in the low- or high-redshift bin when splitting into two subsamples by  $\Sigma_1$  value, which is  $4.3\sigma/1.7\sigma$  ( $5.7\sigma/4.0\sigma$ ). We note that  $\Delta\overline{\text{BHAR}}/\Delta f_{\text{AGN}}$  associated with  $\Sigma_1$  in the SF BD sample is more significant than that associated with  $\Sigma_e$  (see Section 3.2.1). However, we still cannot conclude whether  $\Sigma_1$  or  $M_*$  plays a more fundamental role here, as high- or low- $M_*$  subsamples also have significant  $\Delta\overline{\text{BHAR}}/\Delta f_{\text{AGN}}$  (see Section 3.2.1), and the sample size of SF BD galaxies is too small to disentangle the relative roles of  $M_*$  and  $\Sigma_1$  effects.

We also performed PCOR analyses to test the significance level of the  $\overline{\text{BHAR}}$ –SFR relation when controlling for  $\Sigma_1$ , and the significance level of the  $\overline{\text{BHAR}}$ – $\Sigma_1$  relation when controlling for SFR in the BD sample. The results are summarized in Table 3. The  $\overline{\text{BHAR}}$ – $\Sigma_1$  relation is not significant when controlling for SFR for bulge-dominated galaxies.

### 3.3.2 How does BH growth relate to $\Sigma_1$ for galaxies that are not bulge-dominated?

In Figs 14 or 16, we plot  $\overline{\text{BHAR}}$  as a function of  $M_*$  and  $\Sigma_1$  for galaxies in the Non-BD or SF Non-BD sample. Each  $M_*/\Sigma_1$  bin is further divided into two subsamples with  $\Sigma_1/M_*$  above or below the median  $\Sigma_1/M_*$ , and the  $\overline{\text{BHAR}}$  values of these subsamples are shown on the plot as well. We can see that for both the Non-BD and SF Non-BD samples, differences in  $M_*$  for a given  $\Sigma_1$  (in the right-hand panel) and differences in  $\Sigma_1$  for a given  $M_*$  (in the left-hand



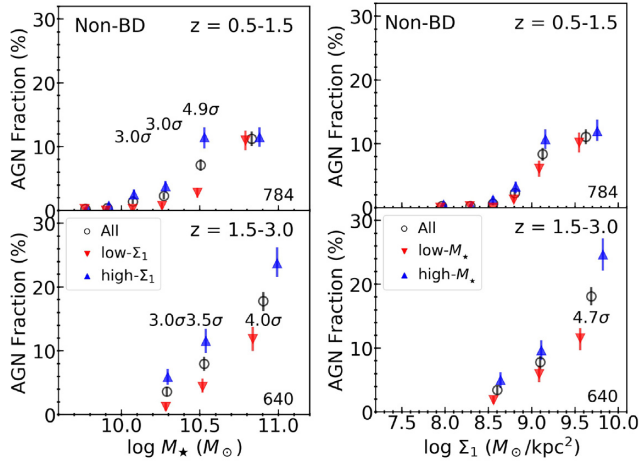


**Figure 15.** AGN fraction versus  $M_*$  (left) and  $\Sigma_1$  (right) for galaxies in the Non-BD sample. The horizontal position of each data point indicates the median  $M_*/\Sigma_1$  (left/right) of the sources in the bin. Each  $M_*/\Sigma_1$  sample (black circles) is further divided into two subsamples with  $\Sigma_1/M_*$  above (blue upward-pointing triangles) and below (red downward-pointing triangles) the median  $\Sigma_1/M_*$  of the sample, respectively. The error bars represent the  $1\sigma$  confidence interval of AGN fraction from bootstrapping. The significance levels of the differences between AGN fraction in the subsamples are labelled at the position of the bin if the level is  $>3\sigma$ . The number in the bottom-right corner represents the number of objects in each  $M_*/\Sigma_1$  bin. Noticeable  $\Delta f_{\text{AGN}}$  values are associated with  $\Sigma_1$  mostly.

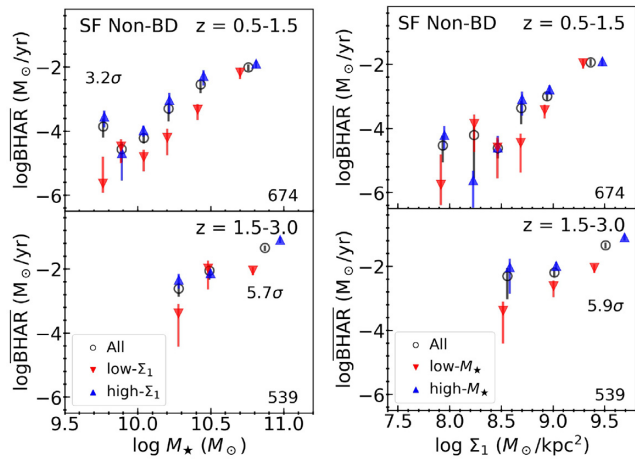


**Figure 16.** Similar to Fig. 14, but for galaxies in the SF Non-BD sample. Noticeable  $\Delta \text{BHAR}$  values are associated with both  $M_*$  and  $\Sigma_1$ .

panel) can both cause noticeable differences in  $\text{BHAR}$ . We also plot AGN fraction as a function of  $M_*$  and  $\Sigma_1$  for galaxies in the Non-BD or SF Non-BD sample in Figs 15 or 17. The bins and subsamples in Figs 15 or 17 are the same as those of Figs 14 or 16. We can see that, for massive galaxies with  $\log M_* \gtrsim 10$  in the left-hand panel of Fig. 15, almost all the mass bins have  $\Delta f_{\text{AGN}}$  associated with  $\Sigma_1$  at a  $\gtrsim 3.0\sigma$  significance level (except for the highest mass bin at  $z = 0.5-1.5$ ), though only two bins satisfy the  $3.6\sigma$  criterion after considering the Bonferroni correction. When we confine the analysis to SF galaxies in the Non-BD sample, the highest mass bin at  $z = 0.5-1.5$  also shows a hint of  $\Delta f_{\text{AGN}}$  (at  $3.0\sigma$ ) associated with  $\Sigma_1$  (see the left-hand panel of Fig. 17). In contrast, significant  $\Delta f_{\text{AGN}}$  associated with  $M_*$  can only be seen in one  $\Sigma_1$  bin (in the right-hand panels of Figs 15 or 17). These results naturally raise

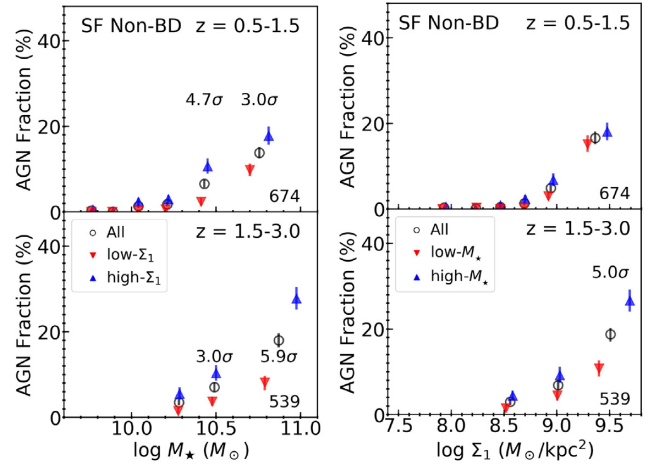


**Figure 17.** Similar to Fig. 15, but for galaxies in the SF Non-BD sample. Noticeable  $\Delta f_{\text{AGN}}$  values are associated with  $\Sigma_1$  mostly.

the question: is the  $\text{BHAR}-\Sigma_1$  relation more fundamental than the  $\text{BHAR}-M_*$  relation for both the Non-BD and SF Non-BD samples?

We then perform PCOR analyses to assess if the  $\text{BHAR}-M_*$  relation is simply a secondary manifestation of the  $\text{BHAR}-\Sigma_1$  relation for both the Non-BD and SF Non-BD samples. We bin sources based on  $M_*$  and  $\Sigma_1$ , and use the median  $\log M_*$ , median  $\log \Sigma_1$ , and  $\log \text{BHAR}$  of each bin as the input to the PCOR analyses. The results are summarized in Table 3. We note that neither the  $\text{BHAR}-M_*$  nor  $\text{BHAR}-\Sigma_1$  relations are significant for both the Non-BD and SF Non-BD samples, probably due to the high level of degeneracy between  $M_*$  and  $\Sigma_1$  (see Fig. 4). Thus, we are not able to conclude which of the  $\text{BHAR}-M_*$  and  $\text{BHAR}-\Sigma_1$  relations is the primary one for the Non-BD or SF Non-BD samples. We further test if the  $\text{BHAR}-C_1$  relation is significant when controlling for  $M_*$ , to determine if BHAR truly depends on  $\Sigma_1$  ( $C_1$  is the percentage of mass concentrated in the central 1 kpc and is independent of  $M_*$ ;  $\log C_1 \approx \log \Sigma_1 - \log M_* + \text{Constant}$ , see equations 6 and 7). However, we note that when performing the PCOR analysis between  $\text{BHAR}$ ,  $M_*$ , and  $C_1$ , we will not be able to test if the  $\text{BHAR}-M_*$  relation is a manifestation of the  $\text{BHAR}-\Sigma_1$  relation. As can be seen in Table 3, the  $\text{BHAR}-M_*$  relation becomes significant when the influence of  $M_*$  in  $\Sigma_1$  is removed for both the Non-BD and SF Non-BD samples. For the Non-BD sample, the  $\text{BHAR}-C_1$  relation is not significant when controlling for  $M_*$ , suggesting that the  $\text{BHAR}-\Sigma_1$  relation not fundamental in this sample. For the SF Non-BD sample at  $z = 0.5-1.5$ , the  $\text{BHAR}-C_1$  relation is just significant at  $3.0\sigma$  when controlling for  $M_*$ . At the same time, for the SF Non-BD sample at  $z = 1.5-3$ , the  $\text{BHAR}-C_1$  relation is not significant when controlling for  $M_*$ . We present the bins divided by  $M_*$  and  $C_1$  of galaxies in the SF Non-BD sample utilized in the PCOR analyses in Fig. 18, with colour-coded  $\text{BHAR}$ . In the left-hand panel of Fig. 18, we can directly observe apparent  $\text{BHAR}-C_1$  relations for a given  $M_*$  at  $z = 0.5-1.5$ , especially at  $\log M_* > 10$ .

The above results indicate that, at least for the SF Non-BD sample at  $z = 0.5-1.5$ , the  $\text{BHAR}-\Sigma_1$  relation is not likely to be only a secondary manifestation of the  $\text{BHAR}-M_*$  relation. A larger sample will be needed to test if this statement holds indisputably for all redshift ranges, and if the  $\text{BHAR}-\Sigma_1$  relation is indeed more fundamental than the  $\text{BHAR}-M_*$  relation for the SF Non-BD sample. We will further discuss the observed link between BH growth and  $\Sigma_1$  in Section 4.2, and we will also discuss the possibility

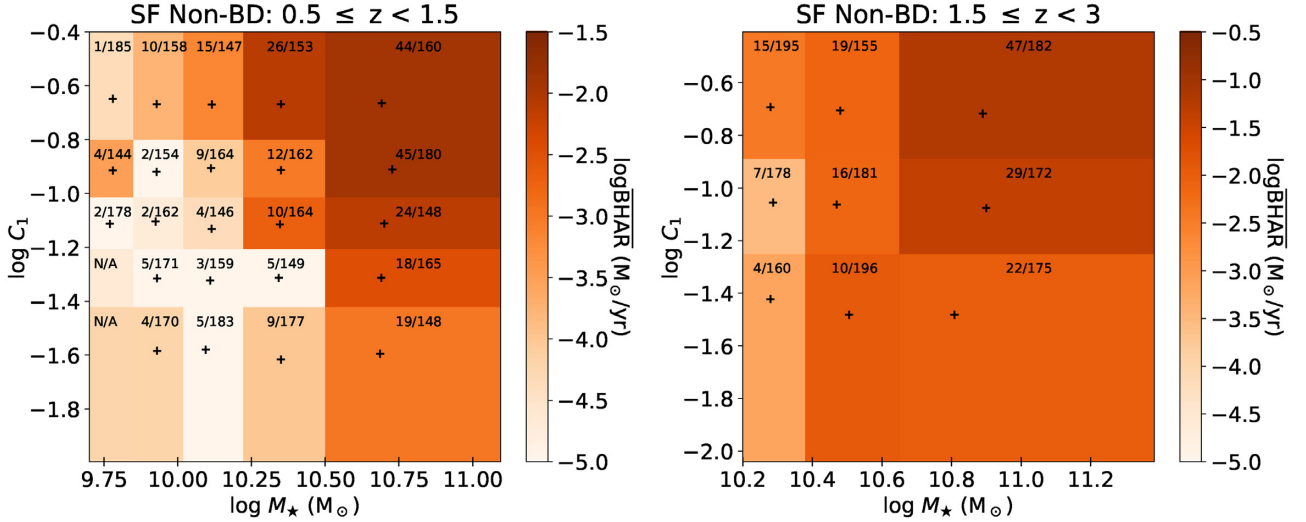


**Figure 18.** Colour-coded  $\overline{\text{BHAR}}$  in different bins of  $M_*$  and  $C_1$  for galaxies in the SF Non-BD sample. The black plus sign indicates the median  $M_*$  and  $C_1$  of the sources in each bin. The median  $\log M_*$ , median  $\log C_1$ , and  $\log \overline{\text{BHAR}}$  are the inputs to our PCOR analyses. For each bin, the number of X-ray detected galaxies and the total number of galaxies are listed. For bins where  $\overline{\text{BHAR}}$  does not have a lower limit  $>0$  from bootstrapping, ‘N/A’ is shown instead. For a given  $C_1$ , the BHAR– $M_*$  relation is overall noticeable, while the BHAR– $C_1$  relation for a given  $M_*$  is more noticeable at  $z = 0.5$ – $1.5$  than at  $z = 1.5$ – $3$ .

that  $\overline{\text{BHAR}}$  only truly depends on  $\Sigma_1$  among massive galaxies (as indicated by Fig. 18) in Section 4.2.3.

## 4 DISCUSSION

### 4.1 The limited power of $\Sigma_e$

In Section 3.2, we found that BH growth does not fundamentally depend on  $\Sigma_e$  in general. In Section 3.2.1, we did not find a fundamental BHAR– $\Sigma_e$  relation when controlling for SFR among galaxies in the BD sample; in Section 3.2.2, we did not find a fundamental BHAR– $\Sigma_e$  relation when controlling for  $M_*$  among galaxies in the Non-BD sample, even when considering only SF galaxies. In Section 4.1.1, we will discuss how these results compare with other results in the literature that have claimed elevated BH growth associated with  $\Sigma_e$ . We will then discuss in Section 4.1.2 the observed potential association between AGN fraction and  $\Sigma_e$  in a characteristic mass range at  $z = 0.5$ – $1.5$  among Non-BD galaxies and the possible reason for it.

#### 4.1.1 Comparison with other results in the literature

A correlation between  $L_X$  and compactness (defined as  $M_*/r_e^{1.5}$ ) has been found in Rangel et al. (2014), utilizing a sample of 268 galaxies with  $M_* > 10^{10.5} M_\odot$  at  $1.4 < z < 3$ . However, the lack of a fundamental link between BHAR and  $\Sigma_e$  (or  $r_e$ ) demonstrated in our work indicates that this correlation is not fundamental. We found in Section 3.2.2 that among Non-BD (or SF Non-BD) galaxies,  $\overline{\text{BHAR}}$  does not significantly depend on  $\Sigma_e$  when controlling for  $M_*$ ; in Appendix B, we found that even when we do not distinguish between BD galaxies and Non-BD galaxies, no fundamental BHAR– $\Sigma_e$  relation is obtained. The above results also hold true when limiting our analyses to galaxies with  $M_* > 10^{10.5} M_\odot$  at  $z = 1.5$ – $3$ . The Rangel et al. (2014) results likely arise due to the dependence of their compactness parameter on  $M_*$ , since  $M_*$  has a strong apparent link with BH growth (e.g. Yang et al. 2017, 2018a).

We also note that in Kocevski et al. (2017), the AGN fraction in massive ‘high- $\Sigma_e$ ’ SF galaxies was found to be significantly higher than that in a mass-matched sample of ‘low- $\Sigma_e$ ’ SF galaxies at  $1.4 < z < 3$ .<sup>8</sup> Given that we find the  $\Delta f_{\text{AGN}}$  association with  $\Sigma_e$  when controlling for  $M_*$  is not significant among SF Non-BD galaxies at  $z = 1.5$ – $3$  (see the lower left-hand panel of Fig. 11), why is elevated BH growth among ‘high- $\Sigma_e$ ’ SF galaxies compared with mass-matched ‘low- $\Sigma_e$ ’ SF galaxies observed in Kocevski et al. (2017)?

We first notice that Kocevski et al. (2017) do not distinguish between bulge-dominated galaxies and galaxies that are not dominated by bulges. We find that we also observe elevated BH growth associated with  $\Sigma_e$  in our sample if we do not distinguish between BD galaxies and Non-BD galaxies. In our  $z = 1.5$ – $3$  sample, 216 SF galaxies satisfy the criterion of being ‘high- $\Sigma_e$ ’ following Kocevski et al. (2017; see our footnote 8 for the Kocevski et al. 2017 definition of ‘high- $\Sigma_e$ ’ galaxies), with median  $\log M_* \approx 10.9$  and median  $\log \Sigma_e \approx 9.7$ . For each of these 216 galaxies, we select one ‘low- $\Sigma_e$ ’ SF galaxy in our  $z = 1.5$ – $3$  sample that has the closest  $M_*$  value to it (not allowing duplications) to constitute a mass-matched ‘low- $\Sigma_e$ ’ sample with median  $\log \Sigma_e \approx 8.9$ . We find that the AGN fraction among these ‘high- $\Sigma_e$ ’ SF galaxies is  $33.3^{+3.3}_{-3.3}\%$ , and the AGN fraction in the mass-matched sample of ‘low- $\Sigma_e$ ’ SF galaxies is  $18.1^{+2.9}_{-2.9}\%$ . The difference in AGN fraction is significant at  $3.5\sigma$ , consistent with the Kocevski et al. (2017) results.

However, if we only consider the 105 of these 216 SF galaxies that are not dominated by bulges (with median  $\log M_* \approx 11.0$  and median  $\log \Sigma_e \approx 9.5$ ), we find that the AGN fraction among these ‘high- $\Sigma_e$ ’ SF Non-BD galaxies is  $28.0^{+4.0}_{-4.0}\%$ , and the AGN fraction in the mass-matched sample of ‘low- $\Sigma_e$ ’ SF galaxies with median  $\log \Sigma_e \approx 8.9$  is  $26.0^{+4.0}_{-4.0}\%$ . The significance of the difference in AGN fraction is only  $0.4\sigma$ , consistent with the limited power of  $\Sigma_e$  presented in Section 3.2.2.

<sup>8</sup>In Kocevski et al. (2017), ‘high- $\Sigma_e$ ’ SF galaxies are SF galaxies that satisfy the relation  $\log \Sigma_e > (-0.52 \times \log M_* - 10.5) + 9.91 - 0.3$ ; ‘low- $\Sigma_e$ ’ SF galaxies are SF galaxies that do not satisfy this relation.

Thus, the high AGN fraction found by Kocevski et al. (2017) among ‘high- $\Sigma_e$ ’ SF galaxies may not be due to high  $\Sigma_e$  values per se, but rather due to the presence of many SF bulges ( $\approx 50\%$ ) which generally have high  $\Sigma_e$  values and high levels of BH growth (e.g. Silverman et al. 2008; Yang et al. 2019). Yang et al. (2019) argue that the high level of BH growth among SF bulges can be explained by the  $\overline{\text{BHAR}}$ –SFR relation among bulge-dominated galaxies. As can be seen in Table 2, for galaxies in the BD sample, the  $\overline{\text{BHAR}}$ –SFR relation is significant, while the  $\overline{\text{BHAR}}$ – $\Sigma_e$  relation is not. Even when only SF bulges are considered, we do not observe a significant difference in  $\overline{\text{BHAR}}$  associated with  $\Sigma_e$  (see Section 3.2.1). These findings further support the idea that, among bulge-dominated galaxies,  $\overline{\text{BHAR}}$  is fundamentally related to SFR rather than  $\Sigma_e$ .

We also note that the correlation between  $L_X$  and compactness found in Rangel et al. (2014) and the elevated BH growth among ‘high- $\Sigma_e$ ’ SF galaxies found in Kocevski et al. (2017) may ultimately reflect a  $\overline{\text{BHAR}}$ – $\Sigma_1$  relation existing among all SF galaxies.<sup>9</sup> We will discuss this  $\overline{\text{BHAR}}$ – $\Sigma_1$  relation for the overall SF galaxy population in Section 4.2.2.

#### 4.1.2 Potential association between AGN fraction and $\Sigma_e$ in a characteristic mass range: the effects of wet compaction events?

The only place where a significant difference in BH growth associated with  $\Sigma_e$  can be seen among Non-BD or SF Non-BD galaxies is for the  $\log M_\star \approx 10.5/10.4$  bin at  $z = 0.5$ – $1.5$  in terms of  $\Delta f_{\text{AGN}}$  (see the left-hand panels of Figs 9 or 11), at  $4.0\sigma/3.7\sigma$ . When using the Bonferroni correction to adjust the required significance level for these  $\Delta f_{\text{AGN}}$  values in Section 3.2.2, we consider the number of tests to be the number of  $M_\star$  bins in the Non-BD or SF Non-BD sample. However, if we are more conservative and treat the number of tests as the total number of  $M_\star$  bins in Figs 6, 8, and 10 (24), we can only call a difference significant if the level is  $> 3.9\sigma$ . In this case, it is less certain that the  $\Delta f_{\text{AGN}}$  associated with  $\Sigma_e$  in a characteristic mass range is not due to statistical fluctuations.

If  $f_{\text{AGN}}$  is indeed associated with  $\Sigma_e$  in this characteristic mass range, this could possibly be explained by a scenario where BH growth is triggered by the high gas density during a wet compaction event (e.g. Wellons et al. 2015; Habouzit et al. 2019), which changes the  $r_e$  of galaxies at the critical halo mass  $M_{\text{halo}} \sim 10^{12} M_\odot$ . It has been suggested that, below the critical halo mass  $M_{\text{halo}} \sim 10^{12} M_\odot$ , supernova feedback is efficient at evacuating the core and BH growth is thus suppressed (e.g. Dekel & Silk 1986; Dekel 2017; Kocevski et al. 2017; Dekel, Lapiner & Dubois 2019). Once the halo reaches the critical mass, the compressed gas during wet compaction events triggered among discs (Dekel & Burkert 2014) can overcome supernova feedback and activate BH growth. After that, the BH continues to grow and regulates the accretion itself. Thus, BH growth will not be linked with  $\Sigma_e$  significantly when  $M_{\text{halo}} \gtrsim 10^{12} M_\odot$ . For  $M_{\text{halo}} \sim 10^{12} M_\odot$ , the corresponding  $M_\star$  is  $\sim 10^{10.4-10.5} M_\odot$  at  $z \approx 0.5$  (e.g. Legrand et al. 2018), which is consistent with the characteristic mass we observed. The corresponding  $M_\star$  is  $\sim 10^{10} M_\odot$  at  $z \approx 2$ , which can also explain why we do not observe significant differences in AGN fraction linked with  $\Sigma_e$  at  $z = 1.5$ – $3$ : our  $M_\star$ -complete sample does not include galaxies with  $\log M_\star < 10.2$  in this redshift range (and we do observe a  $3.2\sigma$  significance for  $\Delta f_{\text{AGN}}$  at  $\log M_\star \approx 10.3$  for the

SF Non-BD sample in Fig. 11). It is not clear from this scenario why the triggered AGNs have low  $L_X$  (as found in Section 3.2.2, the relevant AGNs mainly have  $L_X = 10^{42-43} \text{ erg s}^{-1}$ ). This may be due to the limited gas content at  $z = 0.5$ – $1.5$ .

## 4.2 The relevance of $\Sigma_1$ to BH growth

In Section 3.3.2, we found significant  $\Delta f_{\text{AGN}}$  associated with  $\Sigma_1$  in the Non-BD and SF Non-BD samples at  $z = 0.5$ – $3$  (see Figs 15 and 17), in contrast to the overall non-significant  $\Delta f_{\text{AGN}}$  associated with  $\Sigma_e$  (see Figs 9 and 11). The  $\overline{\text{BHAR}}$ – $C_1$  relation has a  $3.0\sigma$  significance when controlling for  $M_\star$  for the SF Non-BD sample at  $z = 0.5$ – $1.5$  (see Section 3.3.2 and Table 3), suggesting that the  $\overline{\text{BHAR}}$ – $\Sigma_1$  relation is not likely just a secondary manifestation of the primary  $\overline{\text{BHAR}}$ – $M_\star$  relation at least in this regime. In Section 4.2.1, we will discuss the physical implications of this  $\overline{\text{BHAR}}$ – $\Sigma_1$  relation and its possible existence in a broader regime. In Section 4.2.2, we will study the  $\overline{\text{BHAR}}$ – $\Sigma_1$  relation for the overall SF galaxy population when controlling for  $M_\star$ . This is motivated by the discussion in Section 4.2.1 proposing that if the  $\overline{\text{BHAR}}$ –SFR relation of SF BD galaxies is reflecting the same underlying link as the  $\overline{\text{BHAR}}$ – $\Sigma_1$  relation, there is no need to distinguish between SF BD and SF Non-BD galaxies. In Section 4.2.3, we will study the  $\overline{\text{BHAR}}$ – $\Sigma_1$  relation among SF galaxies when  $M_{\text{halo}} \gtrsim 10^{12} M_\odot$ , as theoretical ideas argue that BH growth will be suppressed by supernova feedback when  $M_{\text{halo}} \lesssim 10^{12} M_\odot$ .

### 4.2.1 The $\overline{\text{BHAR}}$ – $\Sigma_1$ relation as a link between BH growth and the central gas density within 1 kpc?

As can be seen in Table 3, the  $\overline{\text{BHAR}}$ – $C_1$  relation has a  $3.0\sigma$  significance for the SF Non-BD sample at  $z = 0.5$ – $1.5$ . For the Non-BD sample in general at  $z = 0.5$ – $1.5$ , the  $\overline{\text{BHAR}}$ – $C_1$  relation is not significant when controlling for  $M_\star$ . This suggestive confirmation of the  $\overline{\text{BHAR}}$ – $\Sigma_1$  relation only among SF galaxies in the Non-BD sample at  $z = 0.5$ – $1.5$  indicates that if the  $\overline{\text{BHAR}}$ – $\Sigma_1$  relation truly exists among SF Non-BD galaxies, it may not be reflecting a link between BH growth and the central stellar-mass density within 1 kpc. Instead, it may reflect a link between BH growth and the central gas density within 1 kpc, with the rough assumption that the  $M_\star$ -to-gas ratios of galaxies are the same. As mentioned in Section 3.1,  $\Sigma_1$  can only serve as an indicator of the central gas density for galaxies that are actively forming stars since when galaxies become quiescent, it is unclear that  $\Sigma_1$  can trace gas conditions.

It is reasonable to speculate that the  $\overline{\text{BHAR}}$ – $\Sigma_1$  relation also exists among SF BD galaxies, as indicated by the significant difference in BH growth associated with  $\Sigma_1$  for such systems (see Section 3.3.1). However, as can be seen in Section 3.2.1, a significant difference in BH growth is also associated with  $M_\star$ , and the current sample size of SF BD galaxies is too small to perform PCOR analyses to disentangle the relative roles of  $M_\star$  and  $\Sigma_1$  effects. If a significant  $\overline{\text{BHAR}}$ – $\Sigma_1$  relation can be confirmed when controlling for both SFR and  $M_\star$  among SF BD galaxies, a straightforward explanation might be found for local BH ‘monsters’ (see Section 1) by attributing their unexpectedly large  $M_{\text{BH}}$  values to elevated BH growth linked with the compactness of host galaxies in the central region. As we discussed before, the  $\overline{\text{BHAR}}$ – $\Sigma_1$  relation could be considered as a manifestation of the link between BH growth and the amount of gas in the vicinity of the central BH. This underlying link may also be the one reflected by the  $\overline{\text{BHAR}}$ –SFR

<sup>9</sup>In the Appendix of Kocevski et al. (2017), they also found elevated AGN fraction associated with  $\Sigma_1$ . However, they did not try to distinguish the relative roles of  $\Sigma_e$  and  $\Sigma_1$  in predicting BH growth.



relation among bulges. Specifically, we know that galaxies in the BD sample are generally compact, with a median  $r_e$  of 1.5/1.1 kpc in the low- or high-redshift bin. Thus, it is possible that the SFR of bulges is substantially correlated with the total amount of cold gas available in the central  $\sim 1$  kpc region, and the  $\overline{\text{BHAR}}$ –SFR relation of bulges is actually a secondary manifestation of an underlying relation between BH growth and the amount of gas in the vicinity of the central BH. When considering the possibility that the  $\overline{\text{BHAR}}$ – $\Sigma_1$  and  $\overline{\text{BHAR}}$ –SFR relations may reflect the same underlying link among SF bulges, there is no need to distinguish between BD and Non-BD galaxies when testing the significance of the  $\overline{\text{BHAR}}$ – $\Sigma_1$  relation among all SF galaxies, and we only need to control for  $M_*$ . We will perform such PCOR analyses for the overall SF galaxy population in Section 4.2.2.

#### 4.2.2 The $\overline{\text{BHAR}}$ – $\Sigma_1$ relation for the overall SF galaxy population

We bin all SF galaxies based on both  $M_*$  and  $\Sigma_1$  (see Fig. 19) to assess if the  $\overline{\text{BHAR}}$ – $\Sigma_1$  relation is more fundamental than the  $\overline{\text{BHAR}}$ – $M_*$  relation when considering all SF galaxies together. We perform PCOR analyses with the median  $\log M_*$ , median  $\log \Sigma_1$ , and  $\log \overline{\text{BHAR}}$  of bins, and the results are summarized in Table 4. We can see that for all SF galaxies at  $z = 0.5$ – $1.5$ , the  $\overline{\text{BHAR}}$ – $\Sigma_1$  relation is significant when controlling for  $M_*$ , and the  $\overline{\text{BHAR}}$ – $M_*$  relation is not significant when controlling for  $\Sigma_1$ . We note that when the bin numbers are reduced from  $5 \times 5$ , neither the  $\overline{\text{BHAR}}$ – $\Sigma_1$  nor  $\overline{\text{BHAR}}$ – $M_*$  relations are significant at a  $3\sigma$  level, but the  $\overline{\text{BHAR}}$ – $\Sigma_1$  relation remains more significant than the  $\overline{\text{BHAR}}$ – $M_*$  relation. For all SF galaxies at  $z = 1.5$ – $3$ , neither the  $\overline{\text{BHAR}}$ – $\Sigma_1$  nor  $\overline{\text{BHAR}}$ – $M_*$  relations are significant. Similar to the approach in Section 3.3.2, we bin sources based on  $M_*$  and  $C_1$  (see Fig. 20) to test if the  $\overline{\text{BHAR}}$ – $C_1$  relation is significant when controlling for  $M_*$ , thus assessing if the  $\overline{\text{BHAR}}$ – $\Sigma_1$  relation can be explained as a secondary manifestation of the primary  $\overline{\text{BHAR}}$ – $M_*$  relation. The median  $\log M_*$ , median  $\log C_1$ , and  $\log \overline{\text{BHAR}}$  of bins are the inputs to the PCOR analyses, and the results are also presented in Table 4. We found that for all SF galaxies at  $z = 0.5$ – $1.5$ , the  $\overline{\text{BHAR}}$ – $M_*$  relation is significant when controlling for  $C_1$ , and the  $\overline{\text{BHAR}}$ – $C_1$  relation is also significant when controlling for  $M_*$ . For all SF galaxies at  $z = 1.5$ – $3$ , the  $\overline{\text{BHAR}}$ – $M_*$  relation is significant when controlling for  $C_1$ , and the  $\overline{\text{BHAR}}$ – $C_1$  relation is not significant when controlling for  $M_*$ . In Section 2.4.3, we mentioned that our results in Section 3 do not change when limiting the analyses to  $H < 23.5$  objects in the sample, where the Sérsic index  $n$  can be measured at the same level of accuracy as  $r_e$  among galaxies with  $H \sim 24.5$  (van der Wel et al. 2012). However, if we confine our sample to  $H < 23.5$  SF galaxies at  $z = 1.5$ – $3$  here ( $\approx 77\%$  of all the SF galaxies at  $z = 1.5$ – $3$ ), the  $\overline{\text{BHAR}}$ – $M_*$  and  $\overline{\text{BHAR}}$ – $C_1$  relations are both significant (see Table 4).

Overall, the results above indicate that the  $\overline{\text{BHAR}}$ – $\Sigma_1$  relation among all SF galaxies is not likely to be a secondary manifestation of the primary  $\overline{\text{BHAR}}$ – $M_*$  relation at  $z = 0.5$ – $3$ , and it is possible that the  $\overline{\text{BHAR}}$ – $M_*$  relation is indeed not fundamental, but a manifestation of the link between BH growth and the central gas density, which can be reflected more effectively by the  $\overline{\text{BHAR}}$ – $\Sigma_1$  relation among SF galaxies.

#### 4.2.3 The $\overline{\text{BHAR}}$ – $\Sigma_1$ relation among SF galaxies when $M_{\text{halo}} \gtrsim 10^{12} M_\odot$

There is suggestive evidence in Section 4.2.2 for the  $\overline{\text{BHAR}}$ – $M_*$  relation being a manifestation of a link between BH growth and

central gas density that can be reflected more effectively by the  $\overline{\text{BHAR}}$ – $\Sigma_1$  relation among SF galaxies. However, we still cannot demonstrate this result confidently, since the only place where the  $\overline{\text{BHAR}}$ – $\Sigma_1$  relation ‘beats’ the  $\overline{\text{BHAR}}$ – $M_*$  relation in the PCOR analyses is for all SF galaxies at  $z = 0.5$ – $1.5$ , and the relation cannot maintain a  $3\sigma$  significance level when the bin numbers are reduced. It is possible that with a larger sample size, we could draw a solid conclusion that the  $\overline{\text{BHAR}}$ – $\Sigma_1$  relation is more fundamental than the  $\overline{\text{BHAR}}$ – $M_*$  relation among SF galaxies; it is also possible that even with a larger sample, we still could not obtain significant results, as  $\Sigma_1$  may only serve as a useful indicator of the central gas density within certain mass ranges according to theoretical proposals (e.g. Dekel & Silk 1986; Dekel et al. 2019). As mentioned in Section 4.1.2, these theoretical ideas argue that when  $M_{\text{halo}} \lesssim 10^{12} M_\odot$ , supernova feedback is effective at evacuating the gas around the central BH, and thus we may not expect  $\Sigma_1$  to serve as a good indicator of the amount of central gas. For SF galaxies at  $z = 1.5$ – $3$ , our limiting  $M_*$  of  $10^{10.2} M_\odot$  already exceeds the  $M_*$  value corresponding to  $M_{\text{halo}} \sim 10^{12} M_\odot$  at  $z \approx 2$  (e.g. Legrand et al. 2018). However, for  $M_{\text{halo}} \sim 10^{12} M_\odot$  at  $z = 0.5$ – $1.5$ , the corresponding  $M_*$  is  $\sim 10^{10.3-10.5} M_\odot$ , which is above our limiting  $M_*$  of  $10^{9.7} M_\odot$  at  $z = 0.5$ – $1.5$ . These theoretical ideas are consistent with our findings in the left-hand panels of Figs 18, 19, and 20, where the  $\overline{\text{BHAR}}$ – $\Sigma_1/C_1$  relation is only apparent among massive SF galaxies at  $z = 0.5$ – $1.5$ .

We thus perform PCOR analyses for all  $\log M_* > 10.3$  (that corresponds to  $M_{\text{halo}} \gtrsim 10^{12} M_\odot$  at  $z \approx 1.5$ ) SF galaxies and SF Non-BD galaxies at  $z = 0.5$ – $1.5$ , where the central gas is not expected to be evacuated by supernova feedback, and thus our assumption of a constant  $M_*$ -to-gas ratio may roughly hold. The results are summarized in Table 5. We found that the  $\overline{\text{BHAR}}$ – $\Sigma_1$  relation is significant when controlling for  $M_*$ , while the  $\overline{\text{BHAR}}$ – $M_*$  relation is not significant when controlling for  $\Sigma_1$ , for both SF galaxies and SF Non-BD galaxies. This clearly suggests that, at least for  $\log M_* > 10.3$  SF galaxies or SF Non-BD galaxies at  $z = 0.5$ – $1.5$ , the  $\overline{\text{BHAR}}$ – $M_*$  relation is a secondary manifestation of the  $\overline{\text{BHAR}}$ – $\Sigma_1$  relation that may reflect a link between BH growth and central gas density.

At the same time, for  $\log M_* \leq 10.3$  SF galaxies or SF Non-BD galaxies at  $z = 0.5$ – $1.5$ , testing shows that neither the  $\overline{\text{BHAR}}$ – $\Sigma_1$  nor  $\overline{\text{BHAR}}$ – $M_*$  relations are significant, which is not a surprise given the limited amount of BH growth at  $\log M_* \leq 10.3$  as can be seen in Figs 18, 19, and 20. With a larger sample of galaxies and AGNs, we can probe if the  $\overline{\text{BHAR}}$ – $\Sigma_1$  relation is more fundamental than the  $\overline{\text{BHAR}}$ – $M_*$  relation among SF Non-BD galaxies in general, or if the  $\overline{\text{BHAR}}$ – $\Sigma_1$  relation is only more fundamental than the  $\overline{\text{BHAR}}$ – $M_*$  relation when  $M_{\text{halo}} \gtrsim 10^{12} M_\odot$ .

## 5 SUMMARY AND FUTURE WORK

We have systematically studied the dependence of BH growth on host-galaxy compactness based on multiwavelength observations of the CANDELS fields. The main points from this paper are the following:

- (i) We have built an  $M_*$ -complete sample of CANDELS galaxies with  $H < 24.5$  and reliable structural measurements at  $z = 0.5$ – $3$  (see Section 2.4.1 and Table 1). We compiled galaxy redshifts,  $M_*$ , SFR,  $r_e$ , and  $n$  from the CANDELS catalogues (see Sections 2.1 and 2.2), and calculated  $\Sigma_e$ ,  $\Sigma_1$ , as well as  $C_1$  (that is independent of  $M_*$ ) to measure the compactness of galaxies (see Section 2.4.3). Based on machine-learning morphological measurements, we construct a

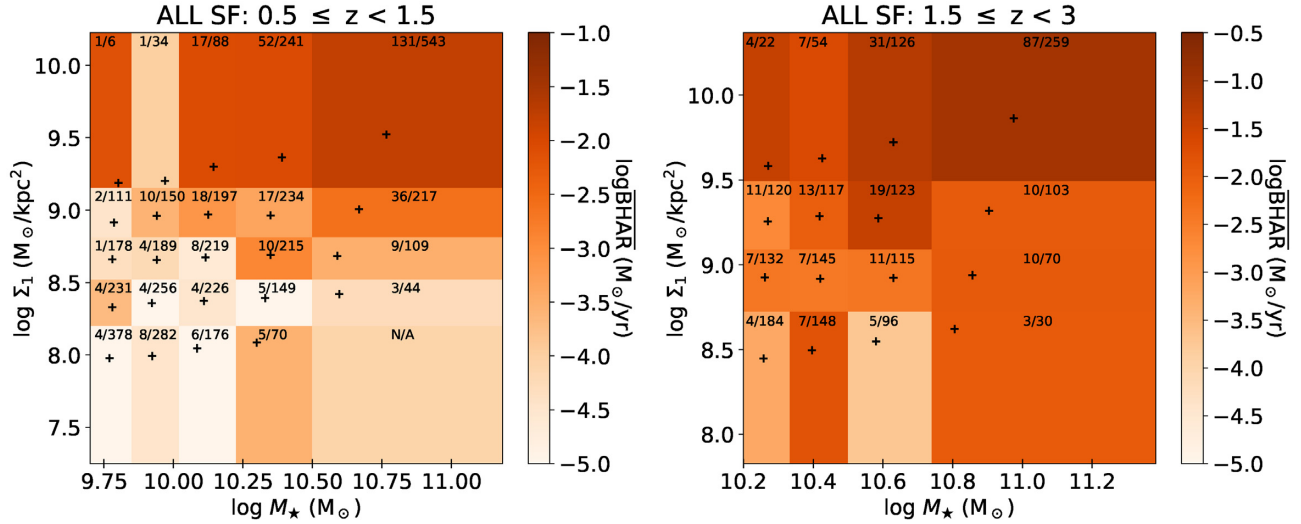


**Figure 19.** Colour-coded  $\overline{\text{BHAR}}$  in different bins of  $M_*$  and  $\Sigma_1$  for all the SF galaxies in the sample. The black plus sign indicates the median  $M_*$  and  $\Sigma_1$  of the sources in each bin. The median  $\log M_*$ , median  $\log \Sigma_1$ , and  $\log \overline{\text{BHAR}}$  are the inputs to our PCOR analyses. For each bin, the number of X-ray detected galaxies and the total number of galaxies are listed. For bins where  $\overline{\text{BHAR}}$  does not have a lower limit  $>0$  from bootstrapping, ‘N/A’ is shown instead. The  $\text{BHAR}-\Sigma_1$  relation is overall more noticeable than the  $\text{BHAR}-M_*$  relation.

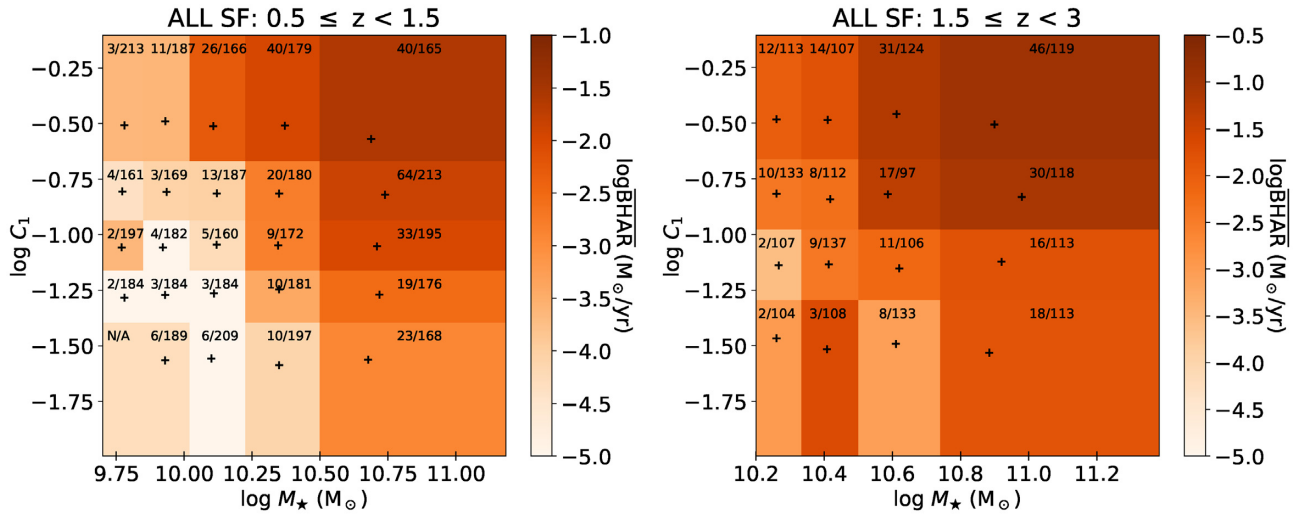


**Figure 20.** Colour-coded  $\overline{\text{BHAR}}$  in different bins of  $M_*$  and  $C_1$  for all the SF galaxies in the sample. The black plus sign indicates the median  $M_*$  and  $C_1$  of the sources in each bin. The median  $\log M_*$ , median  $\log C_1$ , and  $\log \overline{\text{BHAR}}$  are the inputs to our PCOR analyses. For each bin, the number of X-ray detected galaxies and the total number of galaxies are listed. For bins where  $\overline{\text{BHAR}}$  does not have a lower limit  $>0$  from bootstrapping, ‘N/A’ is shown instead. Both the  $\text{BHAR}-M_*$  and the  $\text{BHAR}-C_1$  relations are noticeable.

bulge-dominated sample (the BD sample) and a sample of galaxies that are not dominated by bulges (the Non-BD sample) from the  $M_*$ -complete sample. We also select SF galaxies in these samples (see Section 2.4.2). We utilized deep X-ray observations from *Chandra* to calculate BHAR for relevant subsamples of galaxies, thereby estimating the long-term average BH growth (see Section 2.3).

(ii) We found that  $\overline{\text{BHAR}}$  does not fundamentally depend on  $\Sigma_e$  in general (see Section 3.2 and Table 2). For galaxies in the BD sample,  $\overline{\text{BHAR}}$  does not significantly depend on  $\Sigma_e$  when controlling for SFR (see Section 3.2.1). For galaxies in the Non-BD sample,  $\overline{\text{BHAR}}$  does not significantly depend on  $\Sigma_e$  when controlling for  $M_*$  (see Section 3.2.2); when testing is confined to SF Non-BD galaxies, the  $\overline{\text{BHAR}}-\Sigma_e$  relation is also not significant (see Table 2). Our results indicate that the apparent  $\overline{\text{BHAR}}-\Sigma_e$  relation

is not fundamental, even for the overall SF galaxy population (see Appendix B). We relate our results to other results in the literature claiming elevated BH growth associated with  $\Sigma_e$  in Section 4.1.1.

(iii) We found that the current samples do not reveal a significant  $\overline{\text{BHAR}}-\Sigma_1$  relation among galaxies in the BD or Non-BD sample when controlling for SFR or  $M_*$  (see Section 3.3 and Table 3). However, when testing is confined to SF Non-BD galaxies, we found a just significant ( $3.0\sigma$ )  $\overline{\text{BHAR}}-C_1$  relation when controlling for  $M_*$  at  $z = 0.5-1.5$ . This indicates that the  $\overline{\text{BHAR}}-\Sigma_1$  relation is not simply a secondary manifestation of the primary  $\overline{\text{BHAR}}-M_*$  relation, at least in this redshift range (see Section 3.3.2). For the overall SF galaxy population, we found not only a significant  $\overline{\text{BHAR}}-C_1$  relation when controlling for  $M_*$  at  $z = 0.5-1.5$ , but also suggestive evidence of a significant  $\overline{\text{BHAR}}-C_1$  relation when

**Table 4.**  $p$ -values (significances) of partial correlation analyses for the BHAR– $\Sigma_1$  relation among SF galaxies.

Relation	Pearson	Spearman
All SF Galaxies: $0.5 \leq z < 1.5$ ( $5 \times 5$ bins)		
$\overline{\text{BHAR}}-M_*$	0.06 (1.9 $\sigma$ )	0.11 (1.6 $\sigma$ )
$\overline{\text{BHAR}}-\Sigma_1$	$4 \times 10^{-4}$ (3.5 $\sigma$ )	$2 \times 10^{-3}$ (3.1 $\sigma$ )
$\overline{\text{BHAR}}-M_*$	$9 \times 10^{-7}$ (4.9 $\sigma$ )	$4 \times 10^{-6}$ (4.6 $\sigma$ )
$\overline{\text{BHAR}}-C_1$	$9 \times 10^{-5}$ (3.9 $\sigma$ )	$6 \times 10^{-4}$ (3.4 $\sigma$ )
All SF Galaxies: $1.5 \leq z < 3$ ( $4 \times 4$ bins)		
$\overline{\text{BHAR}}-M_*$	0.42 (0.8 $\sigma$ )	0.31 (1.0 $\sigma$ )
$\overline{\text{BHAR}}-\Sigma_1$	$9 \times 10^{-3}$ (2.6 $\sigma$ )	0.05 (2.0 $\sigma$ )
$\overline{\text{BHAR}}-M_*$	$2 \times 10^{-3}$ (3.1 $\sigma$ )	$6 \times 10^{-3}$ (2.8 $\sigma$ )
$\overline{\text{BHAR}}-C_1$	$7 \times 10^{-3}$ (2.7 $\sigma$ )	0.02 (2.3 $\sigma$ )
All SF Galaxies: $1.5 \leq z < 3$ and $H < 23.5$ ( $4 \times 4$ bins)		
$\overline{\text{BHAR}}-M_*$	0.25 (1.1 $\sigma$ )	0.09 (1.7 $\sigma$ )
$\overline{\text{BHAR}}-\Sigma_1$	0.02 (2.3 $\sigma$ )	0.02 (2.3 $\sigma$ )
$\overline{\text{BHAR}}-M_*$	$1 \times 10^{-4}$ (3.9 $\sigma$ )	$7 \times 10^{-5}$ (4.0 $\sigma$ )
$\overline{\text{BHAR}}-C_1$	$2 \times 10^{-4}$ (3.7 $\sigma$ )	$1 \times 10^{-4}$ (3.8 $\sigma$ )

**Table 5.**  $p$ -values (significances) of partial correlation analyses for the  $\overline{\text{BHAR}}-\Sigma_1$  relation among SF galaxies with  $\log M_* > 10.3$  at  $z = 0.5-1.5$ .

Relation	Pearson	Spearman
All SF Galaxies: $0.5 \leq z < 1.5$ , $\log M_* > 10.3$ ( $4 \times 4$ bins)		
$\overline{\text{BHAR}}-M_*$	0.74 (0.3 $\sigma$ )	0.58 (0.6 $\sigma$ )
$\overline{\text{BHAR}}-\Sigma_1$	$2 \times 10^{-5}$ (4.3 $\sigma$ )	$3 \times 10^{-6}$ (4.6 $\sigma$ )
SF Non-BD: $0.5 \leq z < 1.5$ , $\log M_* > 10.3$ ( $4 \times 4$ bins)		
$\overline{\text{BHAR}}-M_*$	0.13 (1.5 $\sigma$ )	0.14 (1.5 $\sigma$ )
$\overline{\text{BHAR}}-\Sigma_1$	$9 \times 10^{-5}$ (3.9 $\sigma$ )	$2 \times 10^{-4}$ (3.7 $\sigma$ )

controlling for  $M_*$  at  $z = 1.5-3$  (see Section 4.2.2 and Table 4), implying the existence of the  $\overline{\text{BHAR}}-\Sigma_1$  relation at high redshift as well. The  $\overline{\text{BHAR}}-\Sigma_1$  relation may indicate a link between BH growth and the central gas density of galaxies. It is possible that the  $\overline{\text{BHAR}}-M_*$  relation among SF Non-BD galaxies is simply reflecting this link, which needs to be tested with a larger sample. The current SF Non-BD sample suggests that, at least for massive galaxies with  $\log M_* > 10.3$  at  $z = 0.5-1.5$ , the  $\overline{\text{BHAR}}-\Sigma_1$  relation is more fundamental than the  $\overline{\text{BHAR}}-M_*$  relation (see Section 4.2.3 and Table 5). Also, a larger SF BD sample is needed to reveal if, for SF bulges, the  $\overline{\text{BHAR}}-\text{SFR}$  relation in Yang et al. (2019) is a manifestation of this link as well, and SFR alone cannot fully indicate the central gas density.

In the future, we plan to measure  $\Sigma_1$  values for a larger galaxy and AGN sample utilizing the *HST* observations in the COSMOS region, to investigate further the role of  $\Sigma_1$  in long-term average BH growth at  $z = 0.5-1.5$ . At the same time, future accumulation of ALMA pointings will enable us to probe the link between BH growth and central gas density directly: the *HST*-like resolution of ALMA can resolve the central regions of galaxies, and the gas mass can be estimated from CO lines or from the dust mass assuming a typical dust-to-gas ratio. We can also compare the central gas density obtained from ALMA with  $\Sigma_1$  to test if  $\Sigma_1$  among SF galaxies indeed serves as a good indicator of the central gas density. In addition, future deep *JWST* and *WFIRST* imaging combined

with deep X-ray observations can help us probe further the relation between BH growth and  $\Sigma_1$  at  $z \approx 1.5-3$  with a much larger sample size and much smaller  $M_{\text{lim}}$ .

## ACKNOWLEDGEMENTS

We thank Guillermo Barro for sharing  $\Sigma_1$  values and Dale Kocevski for helpful advice. QN, GY, and WNB acknowledge support from *Chandra* X-ray Center grant GO8-19076X, NASA ADP grant 80NSSC18K0878, the V.M. Willaman Endowment, and Penn State ACIS Instrument Team Contract SV4-74018 (issued by the *Chandra* X-ray Center, which is operated by the Smithsonian Astrophysical Observatory for and on behalf of NASA under contract NAS8-03060). DMA thanks the Science and Technology Facilities Council (STFC) for support from grant ST/L00075X/1. BL acknowledges financial support from the National Key R&D Program of China grant 2016YFA0400702 and National Natural Science Foundation of China grant 11673010. FV acknowledges financial support from CONICYT and CASSACA through the Fourth call for tenders of the CAS-CONICYT Fund. YQX acknowledges support from the 973 Program (2015CB857004), NSFC-11890693, NSFC-11421303, the CAS Frontier Science Key Research Program (QYZDJ-SSW-SLH006), and K.C. Wong Education Foundation. The *Chandra* Guaranteed Time Observations (GTO) for the GOODS-N were selected by the ACIS Instrument Principal Investigator, Gordon P. Garmire, currently of the Huntingdon Institute for X-ray Astronomy, LLC, which is under contract to the Smithsonian Astrophysical Observatory via Contract SV2-82024.

## REFERENCES

- Aird J., Coil A. L., Georgakakis A., 2018, *MNRAS*, 474, 1225  
 Antonucci R., 1993, *ARA&A*, 31, 473  
 Barden M., Häußler B., Peng C. Y., McIntosh D. H., Guo Y., 2012, *MNRAS*, 422, 449  
 Barger A. J. et al., 2003, *AJ*, 126, 632  
 Barro G. et al., 2017, *ApJ*, 840, 47  
 Barro G. et al., 2019, *ApJS*, 243, 22  
 Beifiori A., Courteau S., Corsini E. M., Zhu Y., 2012, *MNRAS*, 419, 2497  
 Benjamin D. J. et al., 2018, *Nature Hum. Behav.*, 2, 6  
 Bonferoni C., 1936, *Publ. R. Inst. Super. Sci. Econ. Commer. Firenze*, 8, 3  
 Brandt W. N., Alexander D. M., 2015, *A&AR*, 23, 1  
 Chabrier G., 2003, *PASP*, 115, 763  
 Chen C.-T. J. et al., 2013, *ApJ*, 773, 3  
 Cheung E. et al., 2012, *ApJ*, 760, 131  
 Ciotti L., Bertin G., 1999, *A&A*, 352, 447  
 Civano F. et al., 2016, *ApJ*, 819, 62  
 Conselice C. J., 2003, *ApJS*, 147, 1  
 Cooper M. C. et al., 2012, *MNRAS*, 425, 2116  
 Dekel A., 2017, in *Galaxy Evolution Across Time*, Paris, p. 27  
 Dekel A., Burkert A., 2014, *MNRAS*, 438, 1870  
 Dekel A., Silk J., 1986, *ApJ*, 303, 39  
 Dekel A., Lapiner S., Dubois Y., 2019, preprint ([arXiv:1904.08431](https://arxiv.org/abs/1904.08431))  
 Fragos T., Lehmer B. D., Naoz S., Zezas A., Basu-Zych A., 2013, *ApJ*, 776, L31  
 Galametz A. et al., 2013, *ApJS*, 206, 10  
 Grogin N. A. et al., 2011, *ApJS*, 197, 35  
 Guo Y. et al., 2013, *ApJS*, 207, 24  
 Habouzit M. et al., 2019, *MNRAS*, 484, 4413  
 Häußler B. et al., 2007, *ApJS*, 172, 615  
 Hickox R. C., Mullany J. R., Alexander D. M., Chen C.-T. J., Civano F. M., Goulding A. D., Hainline K. N., 2014, *ApJ*, 782, 9  
 Hopkins P. F., Richards G. T., Hernquist L., 2007, *ApJ*, 654, 731  
 Huertas-Company M. et al., 2015, *ApJS*, 221, 8  
 Ilbert O. et al., 2013, *A&A*, 556, A55



Ishibashi W., Fabian A. C., 2017, *MNRAS*, 472, 2768  
Kim S., 2015, *Commun. Stat. Appl. Methods*, 22, 665  
Kirkpatrick A. et al., 2012, *ApJ*, 759, 139  
Kocevski D. D. et al., 2017, *ApJ*, 846, 112  
Kocevski D. D. et al., 2018, *ApJS*, 236, 48  
Koekemoer A. M. et al., 2011, *ApJS*, 197, 36  
Kormendy J., Ho L. C., 2013, *ARA&A*, 51, 511  
Krist J., 1995, in Shaw R. A., Payne H. E., Hayes J. J. E., eds, *ASP Conf. Ser. Vol. 77, Astronomical Data Analysis Software and Systems IV*. Astron. Soc. Pac., San Francisco, p. 349  
Lee B. et al., 2018, *ApJ*, 853, 131  
Legrand L. et al., 2018, *MNRAS*, 486, 5468  
Lehmer B. D. et al., 2016, *ApJ*, 825, 7  
Li F., Gu Y.-Z., Yuan Q.-R., Bao M., He Z.-C., Bian W.-H., 2019, *MNRAS*, 484, 3806  
Liu T. et al., 2017, *ApJS*, 232, 8  
Luo B. et al., 2010, *ApJS*, 187, 560  
Luo B. et al., 2017, *ApJS*, 228, 2  
Lutz D. et al., 2011, *A&A*, 532, A90  
Magnelli B. et al., 2013, *A&A*, 553, A132  
Magorrian J. et al., 1998, *AJ*, 115, 2285  
Marchesi S. et al., 2016, *ApJ*, 817, 34  
Marconi A., Hunt L. K., 2003, *ApJ*, 589, L21  
Merloni A., Heinz S., 2013, in Oswalt T. D., Keel W. C., eds, *Planets, Stars and Stellar Systems Vol. 6*. Springer, Berlin, p. 503  
Merloni A. et al., 2014, *MNRAS*, 437, 3550  
Mullaney J. R., Alexander D. M., Goulding A. D., Hickox R. C., 2011, *MNRAS*, 414, 1082  
Nandra K. et al., 2015, *ApJS*, 220, 10  
Nayyeri H. et al., 2017, *ApJS*, 228, 7  
Netzer H., 2015, *ARA&A*, 53, 365  
Newman J. A. et al., 2013, *ApJS*, 208, 5  
Oliver S. J. et al., 2012, *MNRAS*, 424, 1614  
Peng C. Y., Ho L. C., Impey C. D., Rix H.-W., 2002, *AJ*, 124, 266  
Rangel C. et al., 2014, *MNRAS*, 440, 3630  
Santini P. et al., 2015, *ApJ*, 801, 97  
Sartori L. F., Schawinski K., Trakhtenbrot B., Caplar N., Treister E., Koss M. J., Urry C. M., Zhang C. E., 2018, *MNRAS*, 476, L34  
Silverman J. D. et al., 2008, *ApJ*, 675, 1025  
Silverman J. D. et al., 2010, *ApJS*, 191, 124  
Stalevski M., Ricci C., Ueda Y., Lira P., Fritz J., Baes M., 2016, *MNRAS*, 458, 2288  
Stefanon M. et al., 2017, *ApJS*, 229, 32  
Tacchella S., Dekel A., Carollo C. M., Ceverino D., DeGraf C., Lapiner S., Mand elker N., Primack Joel R., 2016a, *MNRAS*, 457, 2790  
Tacchella S., Dekel A., Carollo C. M., Ceverino D., DeGraf C., Lapiner S., Mand elker N., Primack J. R., 2016b, *MNRAS*, 458, 242  
Taylor-Mager V. A., Conselice C. J., Windhorst R. A., Jansen R. A., 2007, *ApJ*, 659, 162  
van der Wel A. et al., 2012, *ApJS*, 203, 24

van der Wel A. et al., 2014, *ApJ*, 788, 28  
van Dokkum P. G. et al., 2014, *ApJ*, 791, 45  
Wellons S. et al., 2015, *MNRAS*, 449, 361  
Whitaker K. E., van Dokkum P. G., Brammer G., Franx M., 2012, *ApJ*, 754, L29  
Whitaker K. E. et al., 2017, *ApJ*, 838, 19  
Wuyts S. et al., 2011, *ApJ*, 738, 106  
Xue Y. Q. et al., 2010, *ApJ*, 720, 368  
Xue Y. Q., Luo B., Brandt W. N., Alexander D. M., Bauer F. E., Lehmer B. D., Yang G., 2016, *ApJS*, 224, 15  
Yang G. et al., 2016, *ApJ*, 831, 145  
Yang G. et al., 2017, *ApJ*, 842, 72  
Yang G. et al., 2018a, *MNRAS*, 475, 1887  
Yang G., Brandt W. N., Darvish B., Chen C. T. J., Vito F., Alexander D. M., Bauer F. E., Trump J. R., 2018b, *MNRAS*, 480, 1022  
Yang G., Brandt W. N., Alexander D. M., Chen C. T. J., Ni Q., Vito F., Zhu F. F., 2019, *MNRAS*, 485, 3271  
Yuan F., Yoon D., Li Y.-P., Gan Z.-M., Ho L. C., Guo F., 2018, *ApJ*, 857, 121  
Zolotov A. et al., 2015, *MNRAS*, 450, 2327  
Zou F., Yang G., Brandt W. N., Xue Y., 2019, *ApJ*, 878, 11

## APPENDIX A: ADDING GALAXIES WITH GALFIT.FLAG = 1 INTO THE SAMPLE

As explained in van der Wel et al. (2012), GALFIT.FLAG = 1 does not necessarily indicate a bad fit and those results can be used after assessment on an object-by-object basis. The properties of galaxies with GALFIT.FLAG = 1 are listed in Table A1 with those of galaxies with GALFIT.FLAG = 0. We can see that there is no significant bias towards the X-ray detected objects. However, we note that the presence of irregularity is very high among those less-certain fits, which is expected since irregularity can lead to deviations from Sérsic profiles. Thus, we examined if removing galaxies with GALFIT.FLAG = 1 may bias our results.

We visually examined 890 objects in our sample with GALFIT.FLAG = 1 and removed  $\approx 11\%$  of them that have obvious failures in structural measurements. Then, using a sample of 9637 objects ( $\approx 94\%$  of the objects in the  $M_*$ -complete sample), we confirmed that the results throughout the paper do not change qualitatively when this alternative sample is used.

## APPENDIX B: THE RELATION BETWEEN BH GROWTH AND $\Sigma_E$ FOR ALL SF GALAXIES

In this appendix, we study the  $\overline{\text{BHAR}} - \Sigma_E$  relation among all the SF galaxies in the sample regardless of their morphologies. Similar to

**Table A1.** Properties of galaxies with GALFIT.FLAG = 0 and GALFIT.FLAG = 1 at  $z = 0.5 - 1.5/1.5 - 3$ . (1) Sample name. (2) Number of galaxies in the sample. (3) The fraction of galaxies with the presence of irregularity in the sample, defined as galaxies with  $f_{\text{irr}} \geq 1/10$ . (4) The fraction of X-ray detected galaxies in the sample.

Sample (1)	$N_{\text{Galaxies}}$ (2)	$f_{\text{irregularity}}$ (3)	$f_{\text{X-ray Detected}}$ (4)
$0.5 \leq z < 1.5$			
GALFIT.FLAG = 0 ( <i>J</i> -band)	6247	$28.3\%^{+0.6\%}_{-0.6\%}$	$7.4\%^{+0.3\%}_{-0.4\%}$
GALFIT.FLAG = 1 ( <i>J</i> -band)	530	$43.2\%^{+2.1\%}_{-1.9\%}$	$10.6\%^{+1.3\%}_{-1.3\%}$
$1.5 \leq z < 3$			
GALFIT.FLAG = 0 ( <i>H</i> -band)	2595	$54.3\%^{+1.0\%}_{-1.0\%}$	$11.3\%^{+0.6\%}_{-0.6\%}$
GALFIT.FLAG = 1 ( <i>H</i> -band)	360	$72.5\%^{+2.5\%}_{-2.2\%}$	$11.4\%^{+1.7\%}_{-1.7\%}$

**Table B1.**  $p$ -values (significances) of partial correlation analyses for the BHAR– $\Sigma_e$  relation among SF galaxies.

Relation	Pearson	Spearman
All SF Galaxies: $0.5 \leq z < 1.5$ ( $5 \times 5$ bins)		
$\overline{\text{BHAR}}-M_\star$	$1 \times 10^{-4}$ ( $3.9\sigma$ )	$5 \times 10^{-4}$ ( $3.5\sigma$ )
$\overline{\text{BHAR}}-\Sigma_e$	$9 \times 10^{-3}$ ( $2.6\sigma$ )	0.03 ( $2.2\sigma$ )
$\overline{\text{BHAR}}-M_\star$	$2 \times 10^{-7}$ ( $5.2\sigma$ )	$2 \times 10^{-7}$ ( $5.2\sigma$ )
$\overline{\text{BHAR}}-r_e$	0.02 ( $2.4\sigma$ )	0.02 ( $2.3\sigma$ )
All SF Galaxies: $1.5 \leq z < 3$ ( $4 \times 4$ bins)		
$\overline{\text{BHAR}}-M_\star$	$3 \times 10^{-3}$ ( $3.0\sigma$ )	$3 \times 10^{-3}$ ( $3.0\sigma$ )
$\overline{\text{BHAR}}-\Sigma_e$	0.14 ( $1.5\sigma$ )	0.42 ( $0.8\sigma$ )
$\overline{\text{BHAR}}-M_\star$	$9 \times 10^{-4}$ ( $3.3\sigma$ )	$3 \times 10^{-4}$ ( $3.6\sigma$ )
$\overline{\text{BHAR}}-r_e$	0.18 ( $1.3\sigma$ )	0.04 ( $2.0\sigma$ )

the approach in Section 4.2, we bin sources based on both  $M_\star$  and  $\Sigma_e$ , and calculate  $\overline{\text{BHAR}}$  for each bin to perform PCOR analyses.

We input the median  $\log M_\star$ , median  $\log \Sigma_e$ , and  $\log \overline{\text{BHAR}}$  of bins into PCOR.R to calculate the significance level of the  $\overline{\text{BHAR}}-M_\star$  relation when controlling for  $\Sigma_e$  and the significance level of the  $\overline{\text{BHAR}}-\Sigma_e$  relation when controlling for  $M_\star$ . The results are shown in Table B1.

For the overall SF galaxy population, we found that  $\overline{\text{BHAR}}$  significantly depends on  $M_\star$  when controlling for  $\Sigma_e$ , and  $\overline{\text{BHAR}}$  does not significantly depend on  $\Sigma_e$  when controlling for  $M_\star$ , indicating that the  $\overline{\text{BHAR}}-\Sigma_e$  relation is not fundamental. We test if BH growth has any additional dependence on  $r_e$  when controlling for  $M_\star$  as well, and the results are also shown in Table B1. The  $\overline{\text{BHAR}}-r_e$  relation is not significant when controlling for  $M_\star$  in any case, suggesting that  $r_e$  is not as closely related to BH growth as  $C_1$ , which combines both  $r_e$  and  $n$  to indicate the central morphology of galaxies.

This paper has been typeset from a  $\text{\LaTeX}$  file prepared by the author.